This paper appears in The International Journal of Robotics Research, 2017.
http://dx.doi.org/10.1177%2F0278364916689139

A Grasp-based Passivity Signature for Haptics-enabled Human-Robot Interaction: Application to Design of a New Safety Mechanism for Robotic Rehabilitation

Seyed Farokh Atashzar[1,3], Mahya Shahbazi[1,3], Mahdi Tavakoli[2], Rajni V. Patel[1,3,4]

Abstract

In this paper, the biomechanical capability of the human upper limb in absorbing physical interaction energy during human-robot interaction is analyzed. The outcome is a graphical map that can quantitatively correlate the extent of grasp pressure and the geometry of interaction to the extent of hand passivity. For this purpose, a user study has been conducted for 11 healthy human subjects to characterize energy absorption capability in their arm and wrist. The above correlation is statistically validated. The identified user-specific *Grasp-based Passivity Signature (GPS) map* can be used as a graphical tool to assess the biomechanical capabilities of the upper limb in absorbing interaction energy. In this paper, the proposed GPS map is utilized in the design of a new stabilizer, for haptic systems, that takes into account the variation in energy absorption during haptic task execution. The goal is to optimize the haptic system fidelity while guaranteeing human-robot interaction stability despite the potential existence of delays and a non-passive environment. The controller is termed *GPS-map Stabilizer*. If the user provides minimum to no energy absorption during interaction, the controller makes the force reflection gate tight to guarantee stability. However, when the user demonstrates high capability in absorbing interaction energy, the controller allows the forces to be reflected. The GPS-map Stabilizer is an alternative for (a) conventional stabilizers of haptic/telerobotic systems, and (b) fixed conservative force limits in rehabilitation systems where patient-robot interaction safety is a crucial requirement. This provides the practical motivation for this work. Experimental results are presented.

Keywords

Human-Robot Interaction, Excess of Passivity, Haptics, Non-passive Environments, Physical Energy Dissipation, Safety and Stability, Rehabilitation Robotics, Telerobotic and Haptic Systems.

List of Acronyms

GPS: Grasp-based Passivity Signature, **FRG function:** Force Reflection Gate function, **NP:** Neural Plasticity, **EOP:** Excess of Passivity, **SOP:** Shortage of Passivity, **HRR:** Haptics-enabled Robotic Rehabilitation, **HTR:** Haptics-enabled Telerobotic Rehabilitation, **PVT:** Programmable Virtual Therapist, **ISP:** Input Strictly Passive, **OSP:** Output Strictly Passive, **INP:** Input Non-Passive, **ONP:** Output Non-Passive, **RAMIS systems:** Robotics-assisted Minimally Invasive Surgical systems, **SPT:** Strong Passivity Theorem, **RG:** Relaxed Grasp , **SG:** Stiff Grasp, **TSPL:** Two-Segment Piecewise Linear, **QIT:** Quick Interpolation Technique, **DOF:** Degrees of Freedom, **SA:** Signed Area.

1 Introduction

1.1 Motivation

Telerobotic and haptic systems have attracted a great deal of interest in the context of medical robotics during the last two decades. Accordingly, in the literature, two major categories for haptics-enabled and telerobotic medical systems have been developed, namely: Robotics-assisted Minimally Invasive Surgical (RAMIS) systems Tavakoli et al. (2005), Westebring-Van Der Putten et al. (2008), Tavakoli et al. (2007), Simorov et al. (2012), and Haptics-enabled Robotic Rehabilitation systems (HRR) Blank et al. (2014), Merians and Fluet (2014), Krebs and Hogan (2006), Kim et al. (2013), Hogan et al. (2006).

One of the major research questions about the use of haptic technology in medicine is "how to optimize the haptic system fidelity (transparency) while guaranteeing safety and stability of physical human-robot interaction". An ideally transparent haptic system is capable of providing the user (at the master side) with the kinesthetic feel of force equal to that measured/calculated at the actual/virtual environment side. The case of an actual environment is for telerobotic systems and the case of a virtual environment is for virtual-reality based haptic rendering systems. However, there is a trade-off between stability and ideal transparency in haptic systems.

For RAMIS systems, although the contribution of haptic feedback during surgery is not negligible, this feedback is

[1]Department of Electrical and Computer Engineering, University of Western Ontario, Canada
[2]Department of Electrical and Computer Engineering, University of Alberta, Canada
[3]Canadian Surgical Technologies and Advanced Robotics (CSTAR), Canada
[4]Department of Surgery, University of Western Ontario, Canada

Corresponding author:
S. Farokh Atashzar,
CSTAR, London Health Sciences Centre, University Hospital,
339 Windermere Road, London, Ontario, Canada, N6A 5A5.
Email: satashza@uwo.ca

turned off in most of the currently-available commercial systems Marcus et al. (2015), Okamura (2004). One of the main reasons for the above-mentioned exclusion is to relax the safety/stability concern by avoiding the closed-loop system which would exist if haptic feedback is included. There are also other reasons for excluding this feedback in RAMIS systems, such as cost and concerns about bio-compatibility and size of sensors Okamura (2004), Lendvay et al. (2013). The lack of haptic feedback in commercial systems has nevertheless been successful since without haptic feedback, it is still possible to perform the main goal of RAMIS systems which is accurately translating the "motions" of a surgeon's hand inside a patient's body.

In contrast to surgical applications, haptic feedback and kinesthetic interaction are essential key features of robotic rehabilitation systems and cannot be excluded Blank et al. (2014), Merians and Fluet (2014), Krebs and Hogan (2006), Kim et al. (2013), Hogan et al. (2006). This forms the main motivation of this paper which is guaranteeing stability and safety of human-robot interaction during haptic upper-limb motor rehabilitation while preserving system transparency. The results of this study can be used for any haptic/telerobotic system.

In fact, the safety of human-robot interaction in haptics-enabled rehabilitation systems could be a major concern Zhang and Cheah (2015), Morbi et al. (2014), Vitiello et al. (2013), Aguirre-Ollinger et al. (2012). Most post-stroke rehabilitation robots are designed to generate powerful force fields in order to deliver sufficient energy for the required motor therapy while working in contact with *post-stroke patients*. Consequently, instability in the robots can cause serious injuries including bone, joint, and soft tissue damage Zhang and Cheah (2015), Haddadin et al. (2010). As a result, patient-robot interaction safety should be explicitly studied and guaranteed. This is an active line of research since conservative solutions can degrade the performance of robotics-assisted therapeutic systems Zhang and Cheah (2015), Morbi et al. (2014). In most HRR systems, predefined conservative force caps have been utilized as a safety mechanism Kim et al. (2013), Culmer et al. (2010). This can jeopardize system transparency especially when there may be no stability concern (as explained later in this paper).

Based on the above, the authors believe that the kinesthetic biomechanical capabilities of the human upper limb should be studied not only for motor assessment purposes but also to develop optimal stabilizers which can guarantee patient-robot interaction safety while minimizing transparency distortion and maximizing the allowable intensity of the therapeutic impedance.

1.2 Background

HRR systems have been developed to accelerate Neural Plasticity (NP) in the brain through facilitating therapeutic physical interaction of a patient with actual/virtual objects Krebs and Hogan (2006), Kim et al. (2013), Hogan et al. (2006). NP involving brain remodeling in synaptic and non-synaptic manners helps patients to regain some of their lost motor functions Dimyan and Cohen (2011), Takeuchi and Izumi (2013). The effectiveness of HRR systems in accelerating NP have been investigated in several studies Krebs and Hogan (2006), Kim et al. (2013), Hogan et al. (2006). Conventional HRR systems are composed of (a) a powerful haptics-enabled robot, (b) a virtual-reality interface, and (c) a Programmable Virtual Therapist (PVT) software which is responsible for tuning the therapeutic forces and the intensity of kinesthetic interaction Krebs and Hogan (2006), Hogan et al. (2006).

Through the use of PVT software incorporated in HRR systems, assistive and coordinative therapies are usually prescribed in early stages of rehabilitation to accelerate NP. Also, resistive therapy is mostly prescribed in later stages to equalized and strengthen muscular tone Krebs and Hogan (2006), Hogan et al. (2006).

In addition to HRR systems, taking advantage of recent developments in the field of communication and cloud-based computerized systems, there is a tendency towards developing remote cloud-based medical applications and rehabilitation systems Butler et al. (2014),Schwamm et al. (2009), Bae et al. (2013). An example is the recently-developed Haptics-enabled Telerobotic Rehabilitation (HTR) system, proposed by the authors in Atashzar et al. (2015), Atashzar et al. (2012a), Atashzar et al. (2013), Atashzar et al. (2014a), which can deliver supervised haptic therapy to remote areas, replace PVT software of HRR systems by keeping a human therapist in the loop, and augment capabilities of human therapists using robotic technology.

It should be noted that the other major safety challenge which is highlighted for cloud-based HRR and HTR systems is the destabilizing effect of variable communication time delays and non-passive interaction.

Stability concerns in conventional telerobotic systems have been studied in the literature Chawda and O'Malley (2015), Niemeyer and Slotine (2004), Hashtrudi-Zaad and Salcudean (2002). In this regard, several techniques have been developed to guarantee stability of delayed haptic systems Aziminejad et al. (2008), Sun et al. (2014), Chopra et al. (2008), Ryu et al. (2004), Chawda and O'Malley (2015). However, most of these techniques (a) assume that the terminals are passive and the only source of instability is the time delay; (b) try to guarantee stability for a wide range of users regardless of the corresponding biomechanical capabilities; and (c) are specifically developed for communication-induced instabilities.

1.3 Contributions of This Paper

Although, conventional stabilizers have shown good performance in guaranteeing stability of conventional delayed haptic systems, further developments are essential when dealing with nonpassive rehabilitation systems. The reason is that having a disabled patient as the user not only requires further consideration, but also no assumption can be made regarding the capability of the user in dealing with unstable situations. In addition, transparency manipulation needs to be minimized since force-feedback is the key factor for HRR and HTR systems. However, the quality of force feedback would be affected by using conservative force limits and/or by implementing a stabilizers that trade-off transparency in order to guarantee stability for a wide range of users (having different biomechanics).

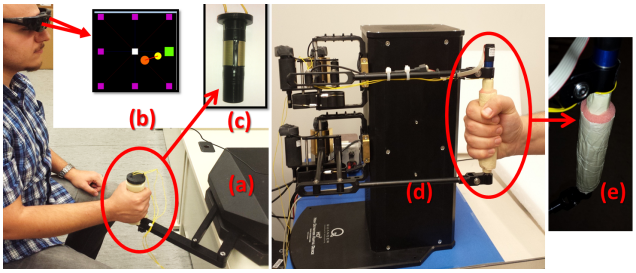

Figure 1. Experimental setup: (a) Quanser upper-limb rehabilitation robot for arm manipulation, (b) virtual environment provided by a head-mounted display, (c) sensorized handle for the arm robot, (d) Quanser HD^2 robot for wrist manipulation, (e) sensorized handle for the wrist robot.

Recently, the authors have shown that it is possible to enhance system transparency and guarantee stability through incorporating some quantitative information of the user's hand biomechanics into the design of the stabilizers Atashzar et al. (2015), Atashzar et al. (2012a), Atashzar et al. (2013). However, in the aforementioned work, a constant lower-bound is considered for the capability of the user's hand in absorbing interactive force and energy.

In this paper, we have relaxed the above-mentioned assumption by proposing a novel Grasp-based Passivity Signature (GPS) map which takes into account the variable energy absorbability of the user's hand during the operation. The presented work has two major contributions:

- Developing the GPS map which correlates the grasp condition and geometry of haptic interaction with the capability of the user's upper limb in absorbing physical interaction energy.
- Proposing a new safety mechanism which incorporates the proposed GPS map to perform minimum manipulation of transparency while guaranteeing stability, in the context of Strong Passivity Theorem (SPT) Vidyasagar (2002), Forbes and Damaren (2010).

For this purpose, in the first part of this work, a user study was conducted with 11 human subjects to study nonlinear biomechanics of both their left and right hands. The study was conducted separately for the users' arms and wrists. Consequently, two haptic systems were utilized: (a) an upper-limb rehabilitation robot (from Quanser Inc., Markham, ON, Canada) for studying arm biomechanics; and (b) an HD^2 haptic device (from Quanser Inc.) for the wrist. The participants were asked to tune their grasp pressure to levels shown by a monitor, while the robot perturbed their limb. Force and motion data were captured and analyzed and the quantitative Excess of Passivity (EOP) was calculated for different directions of motion. Then, the correlation between the calculated EOP (in different geometries of motion) and the amount of grasp pressure was identified and statistically evaluated. The result of this study provides a user-specific GPS map which represents the biomechanical capability of the human upper limb in absorbing interaction energy under variable grasp conditions and in different directions of motion.

In the second part of this work, the identified GPS map was utilized in the design of a new controller, called GPS-map Stabilizer. The proposed technique utilizes the identified user-specific GPS map in a nonlinear Force Reflection Gate (FRG) function, defined to guarantee the interaction safety in the context of SPT. The proposed FRG function can be explained as a nonlinear gain that converges to zero when the user provides minimal to no energy absorption and converges to unity when the user provides enough energy absorption. In the latter case, even if the communication is delayed and the therapy is non-passive (e.g., assistive therapy), the transparency will not be affected by the stabilizer.

It should be noted that the controller can be used not only for HRR/HTR systems but also for conventional haptic and haptic teleoperation systems. Experimental validations are reported to support the proposed technique. The setup is shown Fig. 1.

The rest of this paper is organized as follows. In Section II, the required preliminaries are presented. In Section III, the GPS map is introduced. In Section IV, the design of the proposed FRG function is given. In Section V, experimental evaluations are presented. Finally, concluding remarks are given in Section VI.

2 Preliminaries and Mathematical Modeling

The preliminaries given in this section are mostly taken from the authors' previous work Atashzar et al. (2015). In order to analyze the passivity of the user's hand and develop the stabilizing controller, a transparent two-channel bilateral architecture was previously proposed by the authors Atashzar et al. (2012b) and used for both HRR and HTR systems Atashzar et al. (2015), Atashzar et al. (2012a), Atashzar et al. (2013), Atashzar et al. (2014a). The architecture is an extended version of Lawrence's four-channel model Hashtrudi-Zaad and Salcudean (2001). Using this architecture, it is shown that only two communication channels are needed to allow the patient to feel the delayed therapeutic forces and the human/virtual therapist to feel the patient's delayed hand motion. The details of the utilized telerobotic architecture are in Atashzar et al. (2015). Using the above-mentioned two-channel telerobotic system, transparency is achieved as follows:

$$f_p(t) = -\hat{f}_{th}(t), \tag{1}$$

$$v_{th}(t) = \hat{v}_p(t). \tag{2}$$

In (1), (2), $f_p(t)$ is the force applied by the patient to the master robot, $\hat{f}_{th}(s)$ is the delayed therapeutic force received at the patient's side, sent through the first communication channel (slave to master), $\hat{v}_p(t)$ is the patient's delayed hand velocity, received at the therapist's side, sent through the second communication channel (master to slave). In addition, v_{th} is the therapist-side velocity. Note that for HRR systems v_{th} is the velocity of the virtual object in the virtual reality environment while for HTR systems v_{th} is the velocity of the human therapist. For HRR systems, $\hat{f}_{th}(s)$ is the delayed force generated by the PVT software to deliver assistive/resistive/coordinative therapeutic forces. For HTR systems, $\hat{f}_{th}(s)$ is the delayed force applied by the human therapist on the slave robot.

2.1 Patient's Force Decomposition

The patient's force can be decomposed into an active component $f_p^*(t)$ (which generates movement), and an impeding reactive component $f_{react}(t)$ (which behaves similar to resistive impedance in linear models), as shown below:

$$f_p(t) = f_p^*(t) - f_{react}(t), \text{ where } f_{react} = z_p(v_p, t) \quad (3)$$

In (3), $z_p(v_p,t)$ is the non-autonomous nonlinear impedance function which models the mechanical resistance of the patient's limb. This function relaxes the conventional linearity assumption for the operator's hand dynamics (such as in Tsuji et al. (1995) for a healthy human, and in McCrea et al. (2003) for post-stroke patients). $f_p^*(t)$ is the active component of the force applied by the patient's hand while performing the tasks. $f_p^*(t)$ is composed of (a) residual voluntary (functional) active forces, denoted by $f_{p-v}^*(t)$, and (b) abnormal and involuntary active forces such as abnormal patterns of activation and involuntary reflexes, denoted by $f_{p-i}^*(t)$. Consequently, $f_{p-v}^*(t)$ and $f_{p-i}^*(t)$ result in (a) voluntary, and (b) uncoordinated and involuntary patterns of motion, respectively (Cirstea and Levin (2000); Ellis et al. (2005); Makowski et al. (2015); Sethi et al. (2013)).

The force decomposition can be modeled using the notation of an admittance function $\Omega_p(\cdot)$ as

$$v_p = \Omega_p(f_p^*(t) - f_p(t), t) \quad (4)$$

2.2 Characteristics of the Components of the Interaction

The components of the system have the following characteristics Atashzar et al. (2015).

1. The therapist is considered to be a non-passive nonlinear non-autonomous dynamical terminal for the interconnection. This enables the therapist (virtual/human) to inject energy into the system during assistive and coordinative therapies. The model remains valid during time-varying nonlinear complex therapies.
2. The second norm of the active component of the patient's hand f_p^* is considered to be bounded. This means that the patient can generate positive or negative (voluntary and involuntary) time-varying forces that result in movement; however, the patient does not generate unbounded (in terms of the second norm) forces. This is a realistic assumption.
3. The reaction component of the patient's hand $z_p(v_p,t)$ is *initially* considered as a passive nonlinear non-autonomous biomechanical terminal which absorbs therapeutic energies. This model includes (but is not limited to) the commonly-used passive linear mass-spring-damper models introduced in the literature for the dynamical reaction of a healthy human upper-limb Tsuji et al. (1995), Masia and Squeri (2014), Dyck and Tavakoli (2013) and post-stroke patients McCrea et al. (2003); De Vlugt et al. (2010); Mirbagheri et al. (2008). **In Section 4.1, it is shown that the assumption of passivity on z_p can be relaxed in the proposed framework. This helps to ensure the generality of the technique.**
4. The communication network can be subjected to time-varying delays which is the case for cloud-based HRR and HTR systems and is the conventional source of non-passivity in haptic systems.

The above mentioned considerations are valid for most of the conventional applications of haptic and telerobotic systems including HRR and HTR architectures.

Remark 1. It should be noted that the three common symptoms after stroke are motor weakness, increased joint and muscle resistance to movement (i.e., hypertonia), and increased involuntary reflex activities (De Vlugt et al. (2010); Dietz and Sinkjaer (2007); Thibaut et al. (2013)). The weakness in generating motor commands, will result in reduced ability to move the limbs for performing tasks (e.g., position and/or velocity tracking). Considering (3), this corresponds to a reduced capability in generating $f_{p-v}^*(t)$. Hypertonia results in increasing the viscosity and stiffness of the muscles. Clinicians usually apply movements to the joints to feel the resistance and objectively evaluate hypertonia. As mentioned above, this has been modeled in the literature using linear viscoelastic dynamics, e.g., McCrea et al. (2003); De Vlugt et al. (2010); Mirbagheri et al. (2008). An increase in viscoelastic parameters due to hypertonia increases the magnitude in terms of nonlinear norms of z_p in (3). In addition, the involuntary and abnormal post-stroke muscle activities (such as involuntary reflexive activities and abnormal muscle synergy) result in involuntary forces $f_{p-i}^*(t)$ in (3) and subsequently abnormal involuntary patterns of movement (Cirstea and Levin (2000); Makowski et al. (2015); Sethi et al. (2013); Ellis et al. (2005)). •

Remark 2. It should be noted that in this paper, we *initially* assume the passivity characteristic for the resistive component of the hand dynamics (i.e. z_p). This assumption does not restrict other hand activities such as voluntary and involuntary behavior of the user's hand. In this paper, the only requirement for the active component f_p^* is that the patient should not generate unbounded (in terms of the second norm) active forces, which is realistic. The assumption of passivity on z_p is in agreement with existing linear and passive viscoelastic models which have been used in the literature for modeling limb impedance in post-stroke patients (McCrea et al. (2003); De Vlugt et al. (2010); Mirbagheri et al. (2008)), where increased stiffness and viscosities have been correlated to post-stroke hypertonic symptoms. However, a specifically-designed clinical study is yet to be conducted to provide more details on the passivity characteristics of the impeding component z_p for the upper-limbs (the focus of this paper) of post-stroke patients. Consequently, in order to preserve the generality of the proposed technique and since further investigation may report some non-passive behavior for neurologically-damaged patients (such as the one suggested in Lee and Hogan (2016) for the lower-limb), in Section 4.1 we will show that the assumption of passivity can be relaxed for the proposed framework. •

2.3 Closed-loop system

Utilizing the architecture introduced in the above and detailed in Atashzar et al. (2015), the resulting interconnection for both HTR and HRR is a two-channel closed-loop

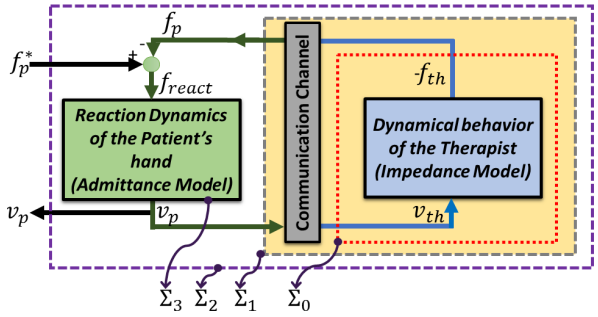

Figure 2. The overall schematic of the resulting interconnection. The subsystem Σ_1 is called the "therapy terminal" which consists of the communication and any behavior of the therapist. Σ_2 is the entire interaction which gets f_p^* as the input and provides v_p as the output. Σ_3 is the admittance model of the patient's limb mechanical reaction.

haptic system which is shown in Fig. 2. The resulting system is an interconnection between (a) the admittance model of the patient's reaction dynamics Σ_3; (b) the impedance model of the therapist's behavior Σ_0; and (c) the communication network. Combination of Σ_0 and the communication network is called "therapy terminal", denoted by Σ_1. Consequently, the resulting system can be summarized as the interconnection of Σ_1 and Σ_3. This enables us to analyze the interaction stability from the perspective of input-output energy exchange between Σ_1 and Σ_3. Note that Σ_1 includes both sources of non-passivity which can destabilize the system (i.e., the delayed communication network and the non-passive therapeutic behaviors). The proposed controller estimates the extent of energy absorption by Σ_3 (using GPS map) and compares it to the energy generated by Σ_1 to tune force reflection parameters and stabilize the system.

2.4 Passivity Definition and EOP-based Stability Condition

When a (virtual/human) therapist provides resistive therapy, they essentially dissipate the energy of the patient's movements. In this case, if the communication is not subject to delays, the situation results in a passive interconnection. However, when the therapist provides assistive/coordinative forces or if the communication network is delayed (which is the case for cloud-based HRR/HTR), the interconnection will be non-passive and can jeopardize the stability of patient-robot interaction Atashzar et al. (2016), Atashzar et al. (2015), Atashzar et al. (2014b). In practice, therapists provide mixed therapies in various time episodes. Also the communication can be delayed. As a result, analyzing the stability in the context of the passivity theorem can allow us to diagnose potential instabilities and provide stabilizing actions through the controller. In this regard, to minimize the transparency distortion and manipulation (commonly used to guarantee stability), we propose to identify the capability of the user's hand reaction dynamics in absorbing energies. Since we do not assume linearity for the limb's dynamics, the passivity is studied in the context of nonlinear control theory and the following definitions are given.

Definition I. *For a system with input vector $u_{in}(t)$, output vector $y_{out}(t)$, and initial energy β at $t=0$, if there exists a constant β such that for all $t \geq 0$ we have*

$$\int_0^t u_{in}(\tau)^T \cdot y_{out}(\tau)\, d\tau \geq \beta, \tag{5}$$

the system is passive Vidyasagar (2002), Jazayeri et al. (2013), Hill and Moylan (1977), Khalil and Grizzle (2002). •

Definition II. *For the system mentioned above, if there is a constant β such that for all $t \geq 0$ we have*

$$\int_0^t u_{in}(\tau)^T \cdot y_{out}(\tau)\, d\tau \geq \beta + \delta \cdot \int_0^t u_{in}(\tau)^T \cdot u_{in}(\tau)\, d\tau, \tag{6}$$

for $\delta \geq 0$, the system is Input Strictly Passive (ISP) with an excess of passivity (EOP) equal to δ. Also, if we have $\delta < 0$, the system is Input Non-Passive (INP) with the Shortage of Passivity (SOP) of δ Vidyasagar (2002), Jazayeri et al. (2013), Hill and Moylan (1977), Khalil and Grizzle (2002). •

Definition III. *For the system mentioned above, if there is a constant β such that for all $t \geq 0$ we have*

$$\int_0^t u_{in}(\tau)^T \cdot y_{out}(\tau)\, d\tau \geq \beta + \xi \cdot \int_0^t y_{out}(\tau)^T \cdot y_{out}(\tau)\, d\tau, \tag{7}$$

for $\xi \geq 0$, the system is Output Strictly Passive (OSP) and the EOP is ξ. If $\xi < 0$, the system is Output Non-Passive (ONP) and the SOP is ξ Vidyasagar (2002), Jazayeri et al. (2013), Hill and Moylan (1977), Khalil and Grizzle (2002). •

Remark 3. It has been shown that all passive systems are asymptotically stable. In addition, an OSP systems is also L_2 stable with a finite L_2 gain less than or equal to $1/\xi$, where ξ is the EOP of the OSP model Khalil and Grizzle (2002). •

Remark 4. In Atashzar et al. (2015), the authors have shown that when there is a nonpassive therapy terminal (Σ_1) in a haptic rehabilitation system (due to a non-passive therapist and/or a non-passive communication network), the closed-loop system Σ_2 can still remain stable if the energy absorbed by the impeding component of the patient's limb (i.e. $\int_0^t f_{react}(\tau)^T \cdot v_p(\tau)\, d\tau$) can compensate for the energy injected by the therapy terminal Σ_1, (i.e. $\int_0^t f_p(\tau)^T \cdot v_p(\tau)\, d\tau$). This condition will be used later in this paper to analyze the stabilizing behavior of the proposed controller. •

Remark 4 can be summarized in the following condition.

$$\text{The entire interconnection } \Sigma_2 \text{ remains passive if } \int_0^t f_p(\tau)^T \cdot v_p(\tau)\, d\tau + \int_0^t f_{react}(\tau)^T \cdot v_p(\tau)\, d\tau \geq 0. \tag{8}$$

This is equivalent to

$$\xi_p + \hat{\delta}_{th} \geq 0, \tag{9}$$

where, ξ_p is the EOP of the patient's hand biomechanics and $\hat{\delta}_{th}$ is the SOP of Σ_1. Details can be found in Atashzar et al. (2015).

Remark 5. The EOP of a human upper limb is the quantitative capability of the corresponding biomechanics in absorbing kinesthetic energy. The more rigid the impeding component of a human upper limb is, the higher the EOP that might be expected. As a result, if a patient has a rigid hand with hypertonia, his/her upper limb might be expected to demonstrate a higher EOP. In the literature higher

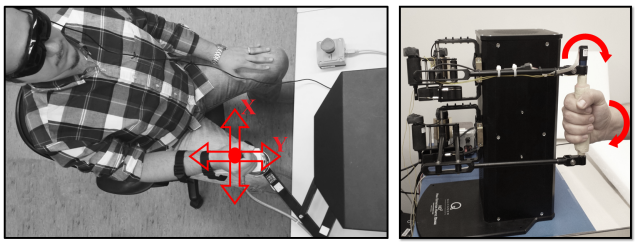

Figure 3. The experimental setup and the resulting motions: (left) Quanser upper-limb rehabilitation robot, (right) Quanser HD^2 robot.

viscoelasticity has been reported for post-stroke patients with hypertonia. High viscoelasticity can mathematically result in high EOP. Clinical analysis is still needed to evaluate this point, as other post-stroke symptoms may affect the result. It should be noted that as discussed in Section 4.1, the assumption on passivity (which results in positive EOP) can be relaxed in the context of the proposed framework. •

If the mentioned passivity condition (8) is not satisfied, some sort of energy manipulation technique should be implemented to compensate for parts of the energy which cannot be absorbed by the EOP of the user's hand. There is no need to compensate for all non-passive therapeutic energies. Consequently, knowledge of the EOP of a user's hand and the corresponding variation and geometry can result in a new stability paradigm which takes into account variable biomechanical capabilities of the user's upper limb in absorbing interaction energies to stabilize the system while performing minimal transparency manipulation.

In this paper, the extent of grasp pressure and the geometry of haptic interaction are correlated with the change in EOP, through the definition of GPS map. This allows us to account for variable grasp-based and geometry-based changes in the capability of the user's upper-limb in absorbing interactive energies, during haptic task execution. The quantified GPS map is then utilized in the design of a new controller (called GPS-map Stabilizer) which modifies the delivered therapeutic energy considering the aforementioned changes in EOP.

3 GPS map Identification and User Study

In this section, the proposed GPS map is introduced and statistically analyzed. For this purpose, the experimental setup shown in Fig. 3 is utilized. For the case of arm interaction, the Quanser upper-limb rehabilitation robot is used to provide 2D planar arm motions composed of elbow flexion-extension, shoulder protraction-retraction and internal-external rotation. In addition, for the case of wrist interaction, the Quanser HD^2 robot is utilized to apply 2D angular wrist movements composed of wrist abduction-adduction and pronation-supination.

3.1 Demographic Data

In order to develop and analyze the proposed GPS map, 11 healthy human subjects were recruited for both the arm and the wrist experiments. Some of the subjects participated in both experiments and some did not. As explained later in this paper, to make each GPS map, two experiments need to be conducted (considering two grasping conditions).

Table 1. Participation Chart for the 40 Calculated GPS maps

ID \ Exp.	Right Wrist Experiment	Left Wrist Experiment	Right Arm Experiment	Left Arm Experiment
P0	✓	✓	✓	✓
P1	✓	✓		
P2	✓	✓	✓	✓
P4	✓	✓	✓	✓
P5	✓	✓	✓	✓
P7	✓	✓	✓	✓
P13			✓	
P15			✓	✓
P16	✓	✓	✓	✓
P17			✓	
P18	✓	✓	✓	
P19	✓	✓		
P20	✓	✓		
P21	✓	✓		
P22			✓	

In total, the participants participated in 80 experiments which resulted in identifying 40 GPS maps. Table 1 shows the participation chart. Note that each item in Table 1 contains two experiments. The study was conducted at the University of Alberta, Canada, under an ethics approval from the corresponding Research Ethics Board. The details of the experiments were explained to the participants prior to the experiment and they were given time to become familiar with the robotic system. For the arm experiment, the participants (6 males, 5 females) were aged between 25 and 30 (mean value: 27.63, standard deviation: 1.36). For the wrist experiment, the participants (8 males, 3 females) were aged between 26 and 40 (mean value: 28.63, standard deviation: 3.93).

3.2 GPS map Identification Protocol

To find the user-specific GPS maps, sinusoidal linear and angular motions were applied to participants' arms and wrists, while force and velocity data were logged. The identifying motion profile was composed of 10 sinusoids with frequencies range from 0 to 2 Hz. It should be noted that 2 Hz is usually considered in the literature as the upper-limit of the frequency range of motion during normal daily activities Herrnstadt and Menon (2016); Taheri et al. (2015). One of the factors which was studied in this paper is the geometry of GPS maps. To account for the geometry, the identifying motion profile was designed in a way that specifically engages different degrees of interaction separately. Consequently, 8 directions of stimulation were considered: $\theta = 0,\ \pi/4,\ \pi/2,\ 3\pi/4,\ \pi,\ 5\pi/4,\ 3\pi/2,\ 7\pi/4$, where θ is the angle of stimulation. The stimulating signal stayed in each of the mentioned 8 phases for 10 seconds and then switched to the next phase. Consequently, the total identification time for one trial was 80 seconds.

For each hand of a participant (right and left) and each limb (wrist and arm), the above-mentioned protocol was conducted two times considering the two different grasp requirements described below. The two aforementioned sets of experiments are denoted as (a) Relaxed Grasp (RG) and

Stiff Grasp (SG) tests. The RG test corresponds to the participant keeping the grasp pressure less than 5% of his/her maximum grasp pressure while the robot is stimulating the limb by applying the motion perturbations. The SG test corresponds to the participant keeping the grasp pressure close to 80% of their maximum grasp during perturbations.

The grasp pressure for each participant was measured using the sensorized robotic handles. The measurement system composed of two FSR-406 (Interlink Electronics) pressure sensors for each robot. Using a head-mounted display, the two levels of grasp pressure (for SG and RG tests) were shown to the participants. Participants were asked to keep the grasp pressure close to the levels shown. Since the experiment was designed such that the participants were not asked to track any trajectory during the identification procedure, they did not apply exogenous kinesthetic forces which means that $f_p^* \rightarrow 0$. Consequently, during the identification procedure we have $\int_0^t f_{react}(\tau)^T \cdot v_P(\tau)\, d\tau = \int_0^t f_p(\tau)^T \cdot v_P(\tau)\, d\tau$, where both $f_p(t)$ and $v_p(t)$ are accessible.

The aforementioned two sets of experiments (SG and RG) were conducted for both the wrist and the arm, and for the left and right hands. As a result, each participant was invited to participate in 8 trials. Out of these 8 trials, four were for the right hand and four for the left hand. Also, out of the mentioned four experiments, two sets (SG and RG) were for the wrist and the other two for the arm. Most of the participants agreed to participate in all 8 trails. In total, 80 experiments were conducted as summarized in Table 1. The results are given in the next subsection. The goal was to identify the GPS map (a) for both the wrist and the arm since it was likely that the GPS map of the wrist and the arm would behave differently in response to the change in the grasp condition; and (b) for both left and right limbs to have a statistically-rich data set.

Remark 6. The study developed in this section addresses the following questions: (a) Is there a statistically significant change in the EOP of the human upper-limb (wrist and arm) under different grasp conditions (realized by the RG and SG tests)? (b) Is the EOP of the human upper-limb (wrist and arm) geometry-specific? As shown later in this paper, the answers to both questions are affirmative and that is why the identified result is denoted as ***GPS map*** for EOP of the human upper-limb. •

Using the collected force and velocity data from each of the 8 identification trials and using the definition of EOP given earlier, the EOP for the participant's limb in the i^{th} direction of stimulation (which corresponds to the i^{th} item of θ), is calculated as

$$\xi_{p-i} = \frac{\int_{Ts_i}^{Te_i} f_{react}(\tau)^T \cdot v_P(\tau)\, d\tau}{\int_{Ts_i}^{Te_i} v_p^T(\tau) \cdot v_P(\tau)\, d\tau}. \qquad (10)$$

In (10), ξ_{p-i} is the estimated EOP of the participant's limb calculated for the i^{th} direction of stimulation, Ts_i is the starting time for stimulating the i^{th} direction, and Te_i is the stop time. The results are given in the following subsection.

3.3 GPS map Identification Results

The results of the proposed GPS map identification protocol are given below. Eight phases of the identification procedure are shown in Fig. 4 for Participant #2, considering the RG test conducted on the right arm. As can be seen in Fig. 4 (a) and (b), force and velocity profiles are collected during 8 phases. Based on the collected data and (10), the EOP of the participant's arm is calculated as given in Fig. 4(c). As can be seen in Fig. 4(c), changing the direction of the stimulation considerably changes the EOP of the participant's hand. In this case, the maximum EOP is 3 times larger than the minimum EOP. Afterwards, the result is transformed to the radarplot of EOP shown in Fig. 4(d). The same procedure is also conducted for the SG test to finally make the complete radarplot (which is the *GPS map*). Consequently, each map includes the geometry of EOP for both the SG and RG tests and represents their graphical summary (which defines the EOP value considering different directions of interaction and levels of grasp pressure). With the 80 experiments that were conducted, 40 GPS maps were made. Fig. 5 shows 15 GPS maps out of the total 40.

Considering the plotted GPS maps in Fig. 5, increasing the grasp pressure results in enlarging the area of EOP in the map. As a result, when a user applies higher grasp pressure, higher energy can be absorbed by their limb. In addition, the EOPs were different in various directions of interaction. The pattern of grasp-based increase and the shape of the EOP area are specific for each participant and each limb. That is why the factor is termed "signature". This information is utilized in the next section to design the GPS-map Stabilizer.

Remark 7. The GPS map of a user's hand can also be potentially used as a graphical representation which has encapsulated information about the user's biomechanical capabilities, and can be studied from the point of view of symmetry, shape and grasp-based size variations. This could be a tool for monitoring progress in strengthening and equalizing muscular functionality, which is critical to assess progress during rehabilitation procedures. •

Remark 8. The order of directions for stimulating the user's biomechanics can be interpreted by comparing Figs. 4(c) and 4(d). In fact in the conducted experiment, during the first phase ($0 < t \leq 10$) the stimulation angle (θ) was 0; for the second phase ($10 < t \leq 20$), we had $\theta = \pi/4$; for the third phase ($20 < t \leq 30$), we had $\theta = \pi/2$; for the fourth phase ($30 < t \leq 40$), we had $\theta = 3\pi/4$; for the fifth phase ($40 < t \leq 50$), we had $\theta = \pi$; for the sixth phase ($50 < t \leq 60$), we had $\theta = 5\pi/4$; for the seventh phase ($60 < t \leq 70$), we had $\theta = 3\pi/2$ and for eighth phase ($70 < t \leq 80$), we had $\theta = 7\pi/4$. Any different order (such as a random one) could be considered for generating GPS maps. The order does not change the entire framework that is proposed in this paper. It should be noted that based on our observations we have not seen correlations between the order, in which the biomechanics of the users were stimulated, and the GPS maps. However, further analysis is needed to scientifically evaluate this point. This forms part of our future study. •

Remark 9. Considering Fig. 4(c), during each phase the identified EOP converges to the corresponding value in less than 5 seconds. This tells us that we may be able to reduce the identification phase to half of what has been tested. In addition, a good suggestion can be to give the user resting

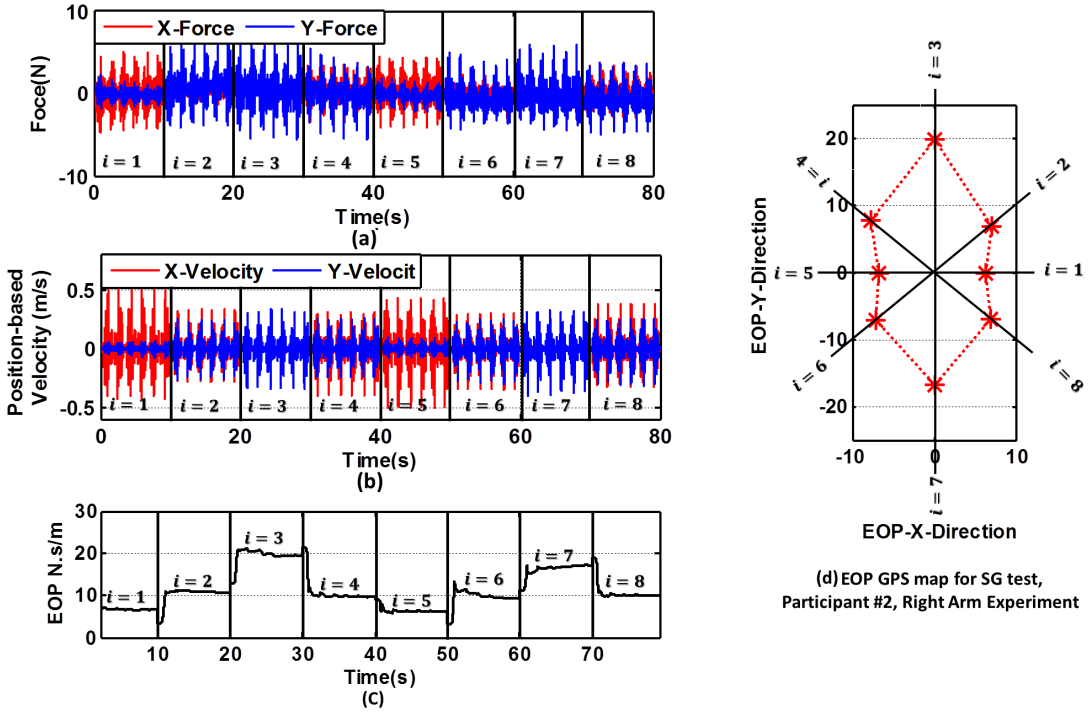

Figure 4. The experimental data for Participant #2, considering RG test on the right arm: (a) force profile, (b) stimulating velocity profile, (c) EOP for 8 phases of the experiment, (d) resulting radarplot.

episodes between every two consecutive phases and evaluate different directions of stimulation with a break in between. This can help to avoid potential fatigue specifically when we ask the user to hold a high grip value. •

3.4 GPS map: Statistical Analysis

This part of the paper focuses on statistical evaluation of the 40 identified GPS maps to analyze them in a more accurate manner. The goal is to illustrate that the correlation between the EOP and (a) grasping condition and (b) geometry of interaction are statistically significant. For this purpose, the following two-step analysis is conducted.

Step #1: The Effect of the Grasping Condition on GPS maps: First, the areas of both radarplots in the GPS maps are calculated. The area for the RG test is denoted by A_{RG} and the area for the SG test is denoted by A_{SG}. The average increase in EOP was calculated for each GPS map as

$$\beta = \sqrt{\frac{A_{SG}}{A_{RG}}} - 1. \tag{11}$$

Note that $\beta = 0$ is equivalent to having zero average increase. In total, forty β values were calculated and the corresponding distributions were developed and analyzed. Note that out of the 40 values, 22 items correspond to the wrist experiments and 18 items correspond to the arm experiments. The results are shown in Fig. 6. As can be seen in Fig. 6, increasing the grasp pressure has increased the EOP of **all the GPS maps** for both the *arm* and the *Wrist*. For the case of the *arm*, the mean value for the increases was 0.82 (that is equivalent to 82% increase in EOP). For this case, the standard deviation was 0.29 (i.e. 29%). For the case of the *wrist*, the mean value for the increases was 3.7 (that is equivalent to 370% increase in EOP). For this case, the standard deviation is 2.26.

Remark 10. In order to statistically analyze the significance of the results obtained, we have conducted standard one-sample *t-test* evaluations on the distributions shown in Fig. 6. A similar approach has also been used for analyzing other results of the paper. The statistical *t-test* evaluation returns a test decision for the null hypothesis that the study data comes from a normal distribution with mean value of zero and unknown variance. The output of the conducted t-test is a *p-value* which is a probability. Small values for p (usually < 0.05) correspond to statistically significant evidence to reject the null hypothesis (Hommel et al. (2009); Seltman (2012)). In this paper, in order to show that the observed positive increases in the area of the calculated GPS maps (resulting from increases in grasp pressure) is statistically significant, we should reject the null hypothesis that the observed changes in the area of the maps comes from a distribution with zero mean increase. A similar approach has also been used for analyzing the effect of geometry on GPS map, in this paper.•

Considering the definitions given in Remark 10, the results of the statistical analyses, that is conducted on the distributions shown in Fig. 6 (**against** $\beta = 0$), are given in Table 2. The results (in Table 2) indicate that the positive average increase in EOP of the participants' arms and wrist (due to increase in grasp pressure) is statistically significant.

Remark 11. Based on the results shown in Table 2, it can be concluded that the increase in grasp pressure considerably increases the EOP of the user's arm and wrist. This was the first hypothesis of the paper which is validated by the above results. The grasp-dependent increase in EOP is statistically significant (p-value$<$0.001) and the average increase is higher for the case of the wrist (i.e., 370%) in comparison to the arm (i.e., 82%). More information about

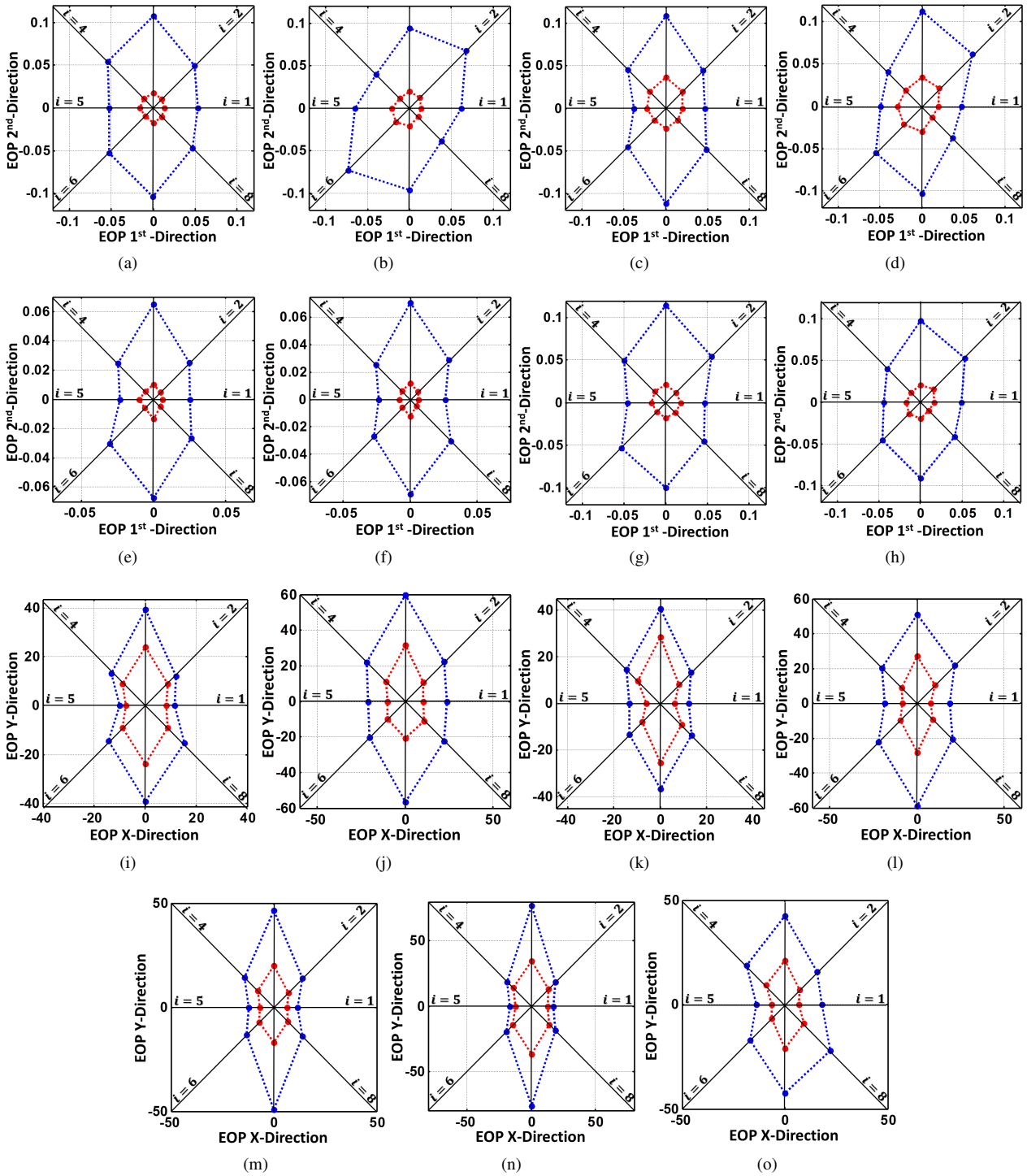

Figure 5. The Calculated GPS maps for 15 items. Note that the blue line corresponds to the SG test and the red line corresponds to the RG test. For the wrist GPS maps, the 1st direction is Pronation-Supination and the 2nd direction is Abduction-Adduction. (a) Participant #18: Right Wrist Experiment, (b) Participant #18: Left Wrist Experiment, (c) Participant #16: Right Wrist Experiment, (d) Participant #16: Left Wrist Experiment, (e) Participant #2: Right Wrist Experiment, (f) Participant #2: Left Wrist Experiment, (g) Participant #0: Right Wrist Experiment, (h) Participant #0: Left Wrist Experiment, (i) Participant #17: Right Arm Experiment, (j) Participant #16: Right Arm Experiment, (k) Participant #7: Right Arm Experiment, (l) Participant #5: Right Arm Experiment, (m) Participant #2: Right Arm Experiment, (n) Participant #0: Right Arm Experiment, (o) Participant #0: Left Arm Experiment,

the results of this statistical analysis (including the t-statistic and degrees of freedom can be found in Table 2). To highlight the importance of the results, it should be noted that an $\alpha\%$ increase in EOP can be transformed to an $\alpha\%$ increase in the allowable amplitude of the force to be reflected to the user's hand which directly enhances the system transparency.•

Step #2: The Effect of Geometry on GPS maps: In the second step, the geometry of GPS maps was separately analyzed for the SG and RG tests and for the cases of the wrist and arm, using the following metric:

$$\gamma = \frac{Max_{EOP}}{Min_{EOP}} - 1. \tag{12}$$

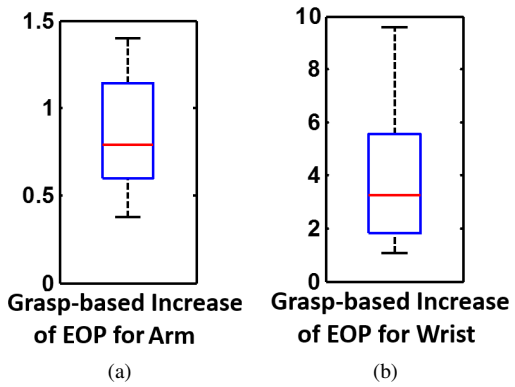

Figure 6. Distributions for grasp-based increase in EOP: (a) Arm, (b) Wrist. In the distributions shown, a sample β value equal to 1 is equivalent to 100% increase in EOP due to increase in grasp pressure.

Table 2. Summary of the Statistical Evaluation for the Distributions Given in Fig. 6. $\beta = 0$ is the value that the t-test is being compared against.

	Mean	Min	Max	Std	t-test result
Arm	0.82	0.38	1.40	0.29	[t(17)= 11.81, p-value<0.001]
Wrist	3.70	1.09	9.60	2.26	[t(21)= 7.65, p-value<0.001]

In (12), Max_{EOP} is the maximum value of the eight EOP values achieved by perturbing the corresponding limb in eight different directions of interaction (i.e., $\theta = 0,\ \pi/4,\ \pi/2,\ 3\pi/4,\ \pi,\ 5\pi/4,\ 3\pi/2,\ 7\pi/4$). Also, Min_{EOP} is the corresponding minimum value. Consequently, in this step, we evaluate the deviation of the GPS map geometries from a circle with a radius equal to Min_{EOP}. In other words, we have evaluated the *anisotropy* of the proposed GPS map using γ. The above-mentioned circle is denoted by "EOP circle" in this paper. In order to evaluate this anisotropy, the distributions of the γ values are analyzed. As a result, four statistical distributions have been calculated namely: (a) SG-Arm, (b) RG-Arm, (c) SG-Wrist and (d) RG-Wrist. Note that the SG-Wrist and RG-Wrist distributions include 22 items and the other two distributions include 18 items. It should be mentioned that $\gamma = 0$ is equivalent to having no geometry-based differences between the calculated EOP values. Also, the higher the γ value, the more deviation from the EOP circle. Consequently, $\gamma = 1$ means that in one direction the EOP is two times larger than Min_{EOP} that results in having two times more capability in absorbing interaction energies. The distributions are shown in Fig. 7. The outcomes of the statistical test conducted on the results given in Fig. 7 **(against $\gamma = 0$)** are given in Table 3.

Remark 12. From the results shown in Fig. 7 and Table 3, it can be concluded that the geometry of stimulation plays an important role in the capabilities of the human hand in absorbing interaction energies. This was our second hypothesis which has been validated using the results given above. In some cases, the EOP can be even more than three times in some directions compared to the minimum EOP. •

Considering Remarks 11 and 12, we have shown that the EOP of the user's hand can be significantly changed by (a) increasing the grasp pressure, and (b) changing the direction of interaction. Consequently, during haptics-enabled task execution, taking advantage of measurable direction of interactive forces and grasp pressure plus the pre-identified GPS map, it is possible to interpolate the expected EOP of the user's hand. This information corresponds to the capability of absorbing interaction energy and can be used to significantly enhance the system transparency while guaranteeing stability. This is accomplished in the next section utilizing the proposed controller, called the *GPS map-Stabilizer*. If the user provides enough EOP, the controller will not undermine the system transparency for preserving stability.

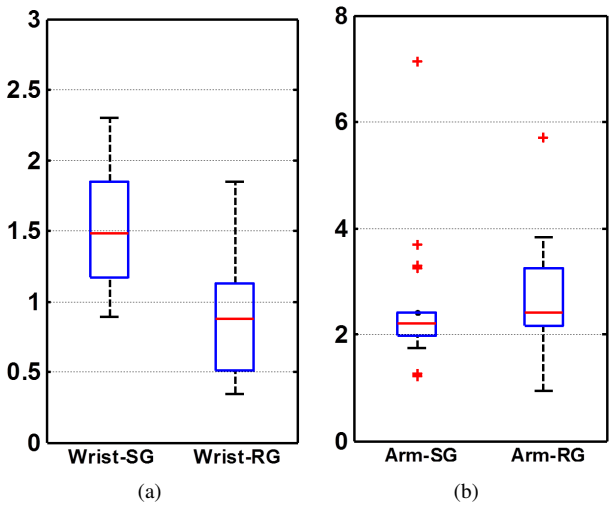

Figure 7. Distribution of geometry-based change in EOP: (a) Wrist, (b) Arm. In the distributions shown, a sample γ value equal to 0 is equivalent to having no geometry-based differences between the calculated EOP values in different directions. The higher the γ value, the more deviation from the EOP circle.

Table 3. Summary of the Statistical Evaluation for the Distributions of γ given in Fig. 7. $\gamma = 0$ is the value that the t-test is being compared against.

	Mean	Min	Max	Std	t-test result
Arm-SG	2.53	1.21	7.13	1.3	[t(17)= 8.16, p-value<0.001]
Arm-RG	2.7	0.94	5.7	1.05	[t(17)= 10.89, p-value<0.001]
Wrist-SG	1.5	0.89	2.3	0.4	[t(21)= 17.34, p-value<0.001]
Wrist-RG	0.87	0.34	1.85	0.42	[t(21)= 9.45, p-value<0.001]

3.5 Case Study: Pattern of Growth in GPS map

In this part of the paper, a case study is presented which focuses on the growth pattern of the introduced GPS maps. The question which is investigated here is *"how to interpolate the EOP value using the proposed GPS maps based on real-time measurement of grasp pressure?"* There are several ways for interpolating the EOP values, in practice.

The most straightforward simple technique is to enrich the GPS map by considering more values for the grasp pressure (called "fractions" in this paper) other than the two values used here (i.e. 5% and 80% of the maximum pressure). An example is a *5-point fractioning technique* which is equivalent to conducting the identification procedure for 5%, 20%, 40%, 60%, and 80% of the maximum grasp pressure. The higher the number of fractions, the more accurate is the interpolation of EOP value. Consequently, this technique suggests that the identification procedure could be repeated for more values of grasp pressure to find a more accurate GPS map. Although, this technique is straightforward, in this section we investigate the possibility of developing a quick interpolation. For this purpose, we have conducted a new set of experiments for 8 participants (*P0, P1, P2, P4, P5, P18, P19, P20*), and for both left and right wrists.

The new set of experiments examines the EOP of the participants' wrists considering the 5-point fractioning technique for their grasp pressure. As a result, we identified the EOP of the participants' wrists for 5%, 20%, 40%, 60%, and 80% of their maximum grasp pressures. For each participant, we individually normalized the calculated EOP using the maximum EOP observed during the 5 stages of the mentioned fractioning. The result of this case study consists of 32 graphs of normalized EOP versus pressure percentage. Each graph contains 5 values of EOP which corresponds to 5%, 20%, 40%, 60%, and 80% of a participant's maximum grasp pressures. The 32 results were obtained by conducting the identification procedure for both right and left wrists of the 8 participants and for both major directions of motion (Supination-Pronation and Abduction-Adduction). Twelve sample graphs are shown in Fig. 8. An interesting phenomenon was observed for all the aforementioned 32 results including the ones which are shown in Fig. 8. The observation is discussed in the following remark.

Remark 13. All 32 results support the fact that the growth pattern of EOP can be modelled using a *"Two-Segment Piecewise Linear (TSPL)"* model. The aforementioned model includes a sharp growth for the first 20% increase in the grasp pressure, and a second linear growth, with a smaller slope, for the next 60% increase in the grasp pressure. The TSPL model is shown by black dashed lines in the graphs of Fig. 8. This pattern can be used to generate the TSPL model by only employing a *3-point fractioning technique* using grasp percentages of 5%, 20% and 80%.

Although the cause of the two-segment piecewise behavior is not the focus of this paper, the authors believe that one possible explanation could be the existence of a dual-stage behavior for the EOP growth pattern. The behavior suggests that increasing the grasp pressure

(A) results in an increase in the antagonistic muscular tone which gradually increases the EOP;
(B) results in a sharp increase due to a sudden forming of a stiff linkage between the high-impedance parts of the hand (located in upper part) and the wrist (which interacts with the robotic handle). This is called locking mechanism in this paper.

Consequently, the dual-stage behavior suggests that the EOP increase which corresponds to the first 20% grasp pressure is affected by both of the above-mentioned points while an increase in EOP beyond 20% is affected mainly by case A (since the linkage is formed by the first 20% of the grasp pressure). More investigations might be needed to better explain the reason. •

Here we study a fast interpolation technique using only a *2-point fractioning technique* as a simple conservative alternative approach to the TSPL technique. The suggested simplified fast scheme is called the *Quick Interpolation Technique (QIT)* in this paper, which considers only the minimum (5%) and maximum (80%) grasp percentages, without using the EOP value for the 20% grasp percentage.

As mentioned earlier, the TSPL model can be used for accurate interpolating the EOP. However, the QIT utilizes a monotonic linear growth for interpolating the EOP value, in a simple but conservative manner. The QIT model is shown by the red dashed lines in Fig. 8. In fact, (a) it represents a linear monotonic behavior to interpolate EOP; (b) it is simpler to implement (compared to the TSPL model) since it only requires two EOP values; (c) it avoids over estimation of the EOP; and (d) it provides a positive confidence margin for the EOP estimation. For some of the results (such as in Fig. 8(g) and 8(k)), the QIT model is very close to the TSPL model and for some others, it provides a higher confidence margin (such as in Fig. 8(d)).

It should be highlighted that "**based on our observations for all 32 results of this case study, the QIT model avoids over estimation of the EOP and can be used for estimating the EOP while providing a confidence margin.**" In order to statistically evaluate the significance and the correctness of the above point, a new statistical analysis was conducted as discussed below.

First, for each user, a polygon shape is constructed using the 5 calculated values of the EOP. The polygons are formed in a plane which has the EOP percentage as the vertical axis and the grasp pressure percentage on the horizontal axis. As a result, on the vertical axis, 0% corresponds to 0 value for EOP and 100% corresponds to maximum observed EOP value for that user. In addition, on the horizontal axis, 0% means 0 grasp pressure and 100% means maximum observed grasp pressure for the user. After making the polygon shapes, we define and calculate a new factor called the "Signed Area (SA)". The magnitude of this factor is the area of the polygon shape normalized by the area of a reference polygon which has 0%, 100% , 100% , 100% , 100% values on the vertical axis for grasp percentages of 5% 20%, 40%, 60% and 80%, respectively. The area of this reference polygon is 3000. The sign of the SA factor is based on the locations of the 5 EOP values with respect to the QIT model. If the EOP values are higher than their QIT-based estimations, the sign is positive. So, the positive sign means that all of the 5 EOP values are higher than those from the QIT model and no over-estimation has occurred. This has been carried out for all 32 results.

In the next step, the statistical distributions of the calculated SAs are created and analyzed using the standard *t-test* technique. The distribution of SAs is shown in Fig 9. The results of the statistical test conducted on the distribution given in Fig. 9 (**against** $SA = 0$) are given in Table 4. As can be seen in Table 4, having a minimum value equal to 0.065 (which has a positive sign) means that no over-estimation has occurred (since no negative SA has been observed). The statistical analysis given in Table 4 shows that the calculated

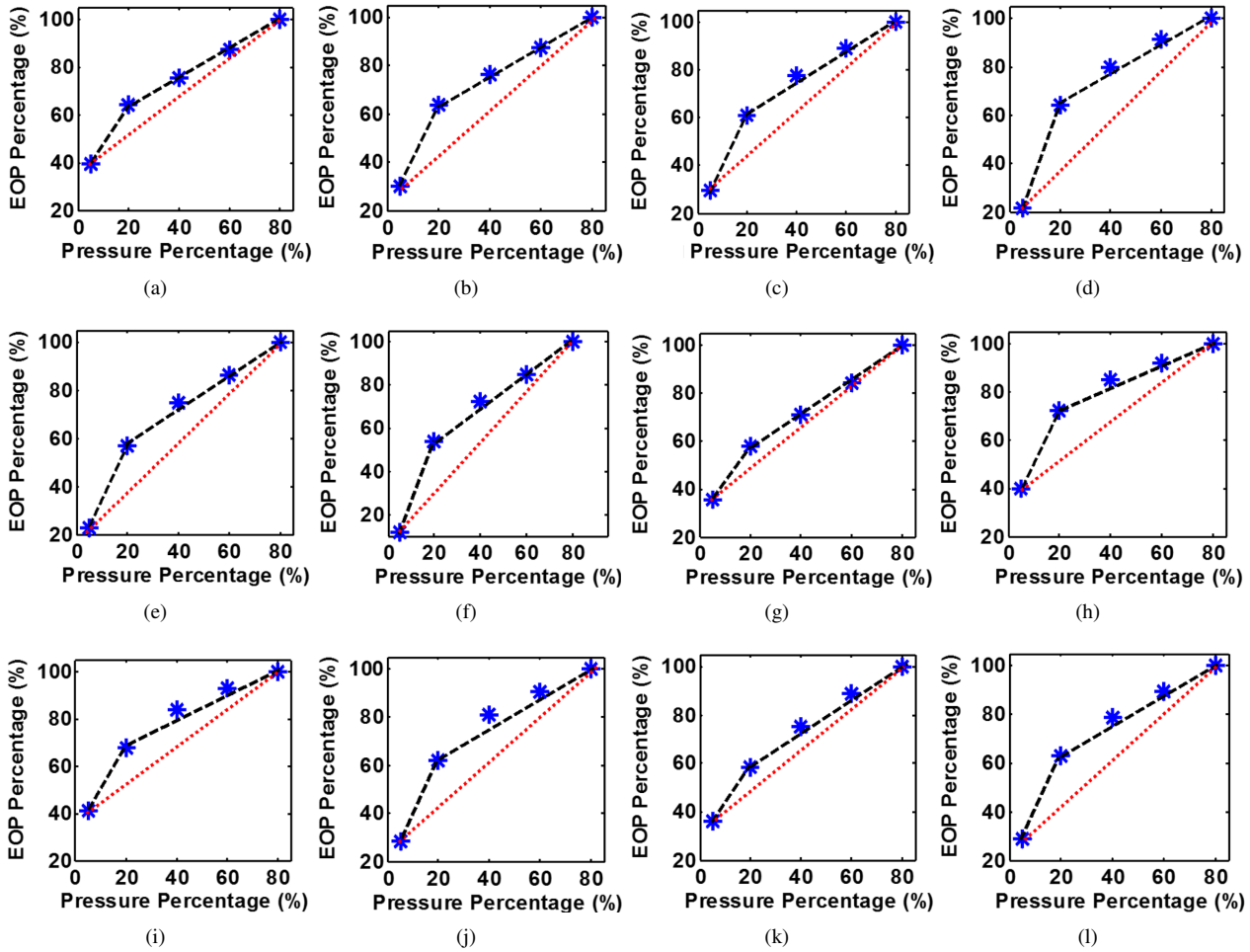

Figure 8. The Calculated EOP percentage versus the grasp pressure percentage. The grasp pressure is normalized using the maximum pressure of the users, and the EOP is normalized by the maximum EOP observed during this experiment. Each graph is made using 5 values. The first dashed black line (on the left) is the linear interpolation for the first 20% of the grasp pressure, and the second dashed black line is the linear interpolation for the last 4 values. The dashed red line is the linear interpolation which can be used for estimating all the values while avoiding over estimation of EOP. This figures includes 12 results out of the 32 results which were calculated. (a) Participant #0: Left Wrist Pronation-Supination, (b) Participant #0: Left Wrist Abduction-Adduction, (c) Participant #20: Right Wrist Pronation-Supination, (d) Participant #20: Right Wrist Abduction-Adduction, (e) Participant #5: Right Wrist Pronation-Supination, (f) Participant #5: Right Wrist Abduction-Adduction, (g) Participant #4: Left Wrist Pronation-Supination, (h) Participant #4: Left Wrist Abduction-Adduction, (i) Participant #1: Left Wrist Pronation-Supination, (j) Participant #1: Left Wrist Abduction-Adduction, (k) Participant #2: Left Wrist Pronation-Supination, (l) Participant #2: Left Wrist Abduction-Adduction,

positive average value for SA is statistically significant. This validates the effectiveness of the QIT model as a fast technique, calculated by using only two grasp conditions, and can conservatively interpolate the EOP while providing a positive confidence margin (i.e., the amplitude of SA).

Remark 14. As can be seen in Fig. 8 the accuracy of the TSPL technique (which includes the EOP value at grasp percentage of 20%) is considerably higher than the QIT model. The reason is the the QIT model does not use any information about the sharp increase in the growth pattern of EOP that occurs during the first 20% increase in grasp pressure. The goal of the study, reported in this part, was only to show that the value of EOP is higher than the one which can be estimated by a monotonic linear growth (QIT model). In other words, the QIT model can provide a conservative estimate of the EOP and avoid over estimation of this value. This has been statistically validated by analyzing the calculated SA values that are indicators of the distance between the QIT model and the TSPL model. It should be added that a statistical curve fitting might be conducted over a population of users to find an average pattern of increase. Although, this can be an interesting investigation, it was not the goal of the reported result. The reason is that an average pattern can lead to considerable over estimation of the EOP value when we only use the relaxed and the stiff grasp conditions. Excessive over estimation of the EOP value is not desirable from the stability point of view for human-robot interaction (as will be clarified in the next section). In summary, in order to estimate the EOP value for an individual for use in the design of the controller, we can either (a) use the three-point/five-point-fractioning technique and generate the TSPL model (which includes the 20% grasp pressure), or (b) use the conservative value suggested by the QIT model that only needs two grasp conditions and does not result in excessive over estimation of the EOP, as supported by the results shown in Table 4. •

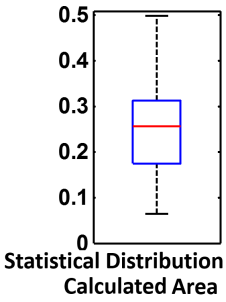

Figure 9. Distribution of the normalized areas calculated for evaluating the QIT model in terms of avoiding over-estimation of EOP by providing positive average SA value.

Table 4. Summary of the Statistical Evaluation for the Distribution of SA given in Fig. 9. $SA = 0$ is the value that the t-test is being compared against

	Mean	Min	Max	Std	t-test result
SA	0.25	0.065	0.5	0.1	[t(31)= 14.2, p-value<0.001]

4 Proposed Stabilizing Control Design: GPS-map Stabilizer

Based on the results shown in the previous section, using real-time measurement of the grasp pressure in addition to the geometry of the received forces at the user's side, it is possible to estimate the EOP of the user's hand through the proposed user-specific GPS map. In this section, the proposed stabilizing scheme is presented which uses the estimated EOP to guarantee stability and enhance transparency. The controller is implemented at the patient's side and is called the *GPS-map Stabilizer*. The main action of the controller is to use the estimated EOP of the user's hand in a *Force Reflection Gate (FRG)* function which changes the loop gain of the system. The FRG function is a time-varying nonlinear force feedback gain which modifies the reflected forces to ensure that the stability condition of the system remains satisfied so the system remains stable and the interaction remains safe. Consequently, if a user represents a low EOP when the delivered therapy is nonpassive (such as assistive therapy), the controller makes the force reflection gate tight to ensure that the amount of delivered nonpassive energy can be absorbed by the user's limb biomechanics to guarantee interaction safety. However, when the user provides higher EOP (which corresponds to the higher capability in absorbing nonpassive energy), the controller opens the gate and allows the forces to be reflected and to be felt more by the user.

After applying the proposed controller, the original close-loop interconnection shown in Fig. 2, is transformed to the one given in Fig. 10. As can be seen in Fig. 10, the controller uses prior knowledge about the GPS map in addition to the real-time measurement of the grasp pressure and the geometry of interaction to calculate the FRG function and tune the loop gain. The proposed controller does not involve a classical additive damping loop; instead, it modifies the amplitude of the reflected forces to guarantee stability while preserving the direction of kinesthetic interaction. This

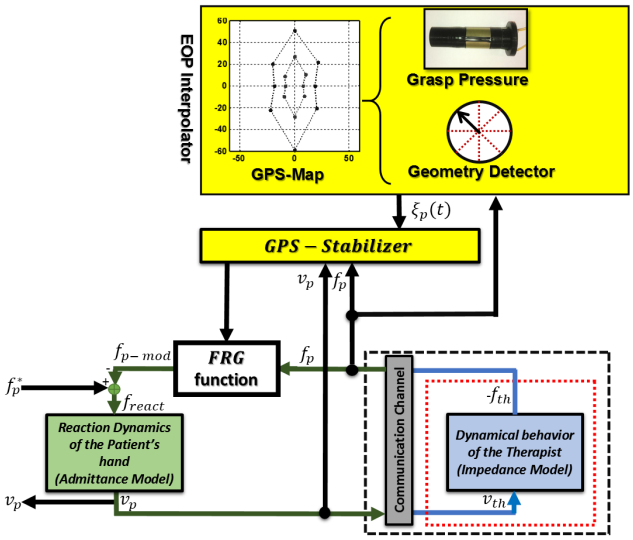

Figure 10. Schematic of the closed-loop interconnection applying the proposed GPS-Stabilizer.

feature is important from a practical consideration and is helpful for enhancing transparency.

Given the estimated EOP of the user's hand $\xi_p(t)$, the functionality of the stabilizer is explained below. Considering the stability condition of the original system (8), applying the controller, the new stability condition is as follows:

$$\textit{The entire interconnection remains passive if:} \quad \int_0^t f_{react}(\tau)^T \cdot v_p(\tau) + f_{p-mod}(\tau)^T \cdot v_p(\tau)\, d\tau \geq 0. \tag{13}$$

In (13), f_{p-mod} is the output of the controller which is the modified force to be reflected. The above stability condition can also be rewritten in a short version as

$$\textit{The entire interconnection remains passive if:} \quad E_p(t) \geq -E_{th-mod}(t). \tag{14}$$

In (14), E_p is the energy that can be absorbed by the biomechanics of the patient's hand and is equal to $\int_0^t f_{react}(\tau)^T \cdot v_p(\tau)\, d\tau$, while E_{th-mod} is the therapeutic energy received at the patient's side after modification by the nonlinear FRG function. Consequently, we have $E_{th-mod}(t) = \int_0^t f_{p-mod}(\tau)^T \cdot v_p(\tau)\, d\tau$. Note that the delivered energy before modification is $E_{th}(t) = \int_0^t f_p(\tau)^T \cdot v_p(\tau)\, d\tau$.

It should be noted that during task execution, $E_{th}(t)$ is measurable; however it is not possible to measure $E_p(t)$ since f_{react} is not accessible when the user performs a task. To design the FRG function, first, assume that $E_p(t)$ is also accessible in real-time. This assumption is relaxed later in this section. Based on the stability conditions (13) and (14), one possible initial design for the FRG function which may guarantee system stability is $f_{p-mod}(t) = \alpha \cdot FRG(f_p, v_p, f_{react})$ where

$$FRG(f_p, v_p, f_{react}) := \begin{cases} f_p(t) & \text{if } f_p(t)^T \cdot v_p(t) \geq 0, \\ \Psi(t) & \text{otherwise.} \end{cases} \tag{15}$$

In (15), we have

$$\Psi(t) = \begin{cases} f_p(t) & \text{if } |f_{react}(t)^T \cdot v_p(t)| \geq |f_p(t)^T \cdot v_p(t)|, \\ ||f_{react}||_2 \cdot \dfrac{f_p(t)}{||f_p(t)||_2} & \text{otherwise.} \end{cases} \tag{16}$$

In (15), α is a positive confidence design factor ($0 \geq \alpha \geq 1$). $\alpha = 1$ defines the maximum gain of the system which can still satisfy the stability condition of the system. $||\cdot||$ represents the 2-norm of a vector.

Through the use of the proposed controller, when the FRG function observes (a) a dissipative power packet $f_p(t)^T \cdot v_p(t) \geq 0$, or (b) a nonpassive packet *which can be absorbed by the user's hand* $|f_{react}(t)^T \cdot v_p(t)| \geq |f_p(t)^T \cdot v_p(t)|$, it does not change the loop gain and allows the power packet to flow. In addition, when the controller observes a non-dissipative power packet, $f_p(t)^T \cdot v_p(t) < 0$, which cannot be absorbed by the user's hand $|f_{react}(t)^T \cdot v_p(t)| < |f_p(t)^T \cdot v_p(t)|$, the proposed FRG function lowers the loop gain to enhance system stability.

As mentioned before, the controller given by (15) assumes that the energy which can be absorbed by the patient's hand (i.e., $E_p(t)$) and the impeding component of the user's hand dynamics f_{react} are accessible measurements. However, in practice, when the user utilizes the robot to perform a task, $f_{react}(t)$ is neither measurable nor accessible. Consequently, it is not possible to directly calculate the energy that can be absorbed by the patient's hand $E_p(t)$ and the corresponding power packets. This issue is addressed by the proposed GPS map which provides an estimate of the energy that can be absorbed by the user's hand. Consequently, instead of using $E_p(t)$ and f_{react} in (16) to calculate $\Psi(t)$, the estimated EOP value provided by the GPS map is utilized and the design of the stabilizing controller is explained below.

First, regarding the passivity condition of the user's hand and considering (7), it can be shown that when the EOP is changing, we have

$$\begin{aligned} \int_0^t f_{react}(\tau)^T v_p(\tau)\, d\tau &\geq \int_0^t \xi_p(\tau) v_P(\tau)^T v_p(\tau)\, d\tau \\ &\geq \xi_{p-min} \int_0^t v_P(\tau)^T v_p(\tau)\, d\tau. \end{aligned} \tag{17}$$

In (17), $\xi_p(t)$ is the varying EOP of the user's hand which can be estimated using the corresponding GPS map. Also, ξ_{p-min} is the minimum value of $\xi_p(t)$. Consequently, considering (17) and (14), the following new stability condition can be obtained:

$$\begin{gathered} \textit{The entire interconnection remains passive if:} \\ \hat{E}_p(t) \geq -E_{th-mod}(t) \\ \text{where } \hat{E}_p(t) = \int_0^t \xi_p(\tau) v_P(\tau)^T v_p(\tau)\, d\tau. \end{gathered} \tag{18}$$

The expanded version of the above stability condition is

$$\begin{gathered} \textit{The entire interconnection remains passive if:} \\ \int_0^t \xi_p(\tau) v_P(\tau)^T v_p(\tau) + f_{p-mod}(\tau)^T \cdot v_p(\tau)\, d\tau \geq 0 \end{gathered} \tag{19}$$

Using the Cauchy-Bunyakovsky-Schwarz inequality and (19), the GPS-map Stabilizer that guarantees system stability can be designed as $f_{p-mod}(t) = \alpha \cdot FRG(f_p, v_p, \xi_p \cdot v_p)$ where

$$FRG(f_p, v_p, \xi_p \cdot v_p) := \begin{cases} f_p(t) & \text{if } f_p(t)^T \cdot v_p(t) \geq 0, \\ \Psi(t) & \text{otherwise.} \end{cases} \tag{20}$$

In (20), we have

$$\Psi(t) = \begin{cases} f_p(t) & \text{if } |\xi_p(t) v_P(t)^T v_p(t)| \geq |f_p(t)^T \cdot v_p(t)|, \\ ||\xi_p(t) v_P(t)||_2 \cdot \dfrac{f_p(t)}{||f_p(t)||_2} & \text{otherwise.} \end{cases} \tag{21}$$

In fact, (20) and (21) define the proposed GPS-map Stabilizer. The technique utilizes the user-specific GPS map to calculate $\xi_p(t)$ and finally tune the loop gain through the proposed nonlinear $FRG(\cdot)$ function, in order to guarantee that the stability condition (19) is satisfied.

Using the proposed GPS-map Stabilizer, the force reflection gate will be tuned in a real-time and the user-specific manner based on the corresponding biomechanical capabilities of the user's hand in absorbing interactive energy. As a result, if a user represents a high EOP (considering the direction of interaction and the grasp pressure), the controller may completely open the force reflection gate and allow the non-passive energy to flow since it can be absorbed by the user's hand biomechanics and will not result in unsafe instability. Consequently, even if the interconnection includes a non-passive communication network and/or non-passive environment, the controller only compensates for a part of non-passive energy which cannot be absorbed by the user's hand at each time instant. The proposed GPS-map Stabilizer takes into account the intensity of grasp pressure and the geometry of interaction together with the user-specific GPS map to find the amount of energy to be compensated for. If the calculated EOP of the user's hand is high-enough, the controller can guarantee a perfectly transparent and stable system regardless of existence of nonpassivity sources.

The proposed GPS-map Stabilizer can be used for any haptic system, including HRR and HTR, to guarantee stability while enhancing transparency. It relaxes the conventional passivity assumption on the behavior of the environment (such as the one made in Albu-Schäffer et al. (2007); Chawda and O'Malley (2015)). The major differences between the proposed GPS-map Stabilizer and conventional state-of-the-art time-domain passivity controllers, designed for haptic systems Hannaford and Ryu (2002), are that the proposed technique (a) takes into account the variable EOP of the user's biomechanics (considering the amount of grasp pressure and the geometry of interaction) in order to take advantage of the existing EOP resources during interaction; and (b) preserves the direction of force feedback in the Cartesian domain which is important from a practical point of view.

4.1 Case Study: Non-passivity of Hand and The GPS-map Stabilizer

In this part, we discuss how the proposed framework can be extended to relax the passivity assumption on the impeding part of the patient's hand. Relaxing the non-passivity assumption for the proposed framework requires some extensions in the design of both the GPS-map visualization technique and the proposed stabilizer. The discussion is divided in two parts:

4.1.1 Part A: Exponential GPS mp (E-GPS map) : Considering the definition given in (7), the extent of passivity

can be either non-negative ($\xi \geq 0$) which is denoted as EOP, or negative which is denoted as SOP in Section 2.4. As a result, by conducting the identification calculation given in (10), if the outcome (i.e., ξ_{p-i}) is non-negative, then we call it EOP. However, if the patient shows a non-passive behavior in some directions of interaction, we will have negative ξ_{p-i} values which is called SOP. The current design of the proposed radar plot of the GPS-map (explained in Section 3.3 and shown in Fig. 4(d) for Participant #2) is based on a non-negative radius value (which shows ξ_{p-i}) and a phase value (which shows the direction of interaction). As a result, negative values for the radius (which correspond to SOP) are not supported by the design of the radar plot shown in Section 3.3.

There are different ways to address this. One is to add a third axis to the visualization of the GPS map which can visualize the negative values. The other technique, explained here is to use a nonlinear one-to-one mapping function which maps the $(-\infty,+\infty)$ window of the extent of passivity to $(0,+\infty)$ window of the transformed one. Here we suggest an exponential mapping. The result is denoted as Exponential GPS map (E-GPS map) which uses the following calculation for $E_{\xi_{p-i}}$ as the radius of its 2D radar plot:

$$E_{\xi_{p-i}} = e^{\xi_{p-i}}. \tag{22}$$

In (22), ξ_{p-i} is the extent of passivity. This value is EOP when it has the positive sign and is SOP when it has the negative sign. ξ_{p-i} is calculated using (10) for the i^{th} direction of stimulation. In addition, $E_{\xi_{p-i}}$ is the radius of the radar plot for the E-GPS map. As a result, $E_{\xi_{p-i}}$ can represent both passive and non-passive limb activities. If a patient shows non-passive limb dynamics in some directions, the E-GPS value in those directions will be inside the unit circle; and if he/she shows passive limb dynamics, the corresponding value in the E-GPS map will be outside of the unit circle. As a result, **the unit circle** represents the border of passivity in the E-GPS map, proposed to visualize both passive and non-passive behavior of a user.

4.1.2 Part B: E-GPS-map Stabilizer : In the next step, we need to relax the passivity assumption for the proposed controller. For this purpose, using the same mathematical approach, as used for (20) and (21), the design of the FRG function is extended as given in (23) and (24).

$$FRG(f_p, v_p, \xi_p \cdot v_p) :=$$
$$\begin{cases} f_p(t) & \text{if } f_p(t)^T \cdot v_p(t) + \xi_p(t) v_P(t)^T v_p(t) \geq 0, \\ \Psi(t) & \text{otherwise.} \end{cases} \tag{23}$$

In (23), we have $\Psi(t) = \mu(t) \cdot \dfrac{f_p(t)}{||f_p(t)||_2}$, where:

$$\mu(t) = \begin{cases} ||\xi_p(t) v_P(t)||_2 & \text{if } \xi_p(t) v_P(t)^T v_p(t) \geq 0, \\ ||\xi_p(t) v_P(t)||_2 & \text{if } f_p(t)^T \cdot v_p(t) \geq 0, \\ 0 & \text{otherwise.} \end{cases} \tag{24}$$

Considering (23) and (24), if the patient has a passive limb impedance ($\xi_p \geq 0$) the designed FRG function behaves as the one designed in (20) and (21). However, the new design covers the case of non-passivity in the patient's hand ($\xi_p <$ 0), as well. The extended stabilizer is denoted as E-GPS-map Stabilizer which utilizes the E-GPS map to observe the extent of passivity at the patient's side. For this purpose, it uses the natural logarithm operator to calculate ξ_p from the E-GPS map of the patient's hand.

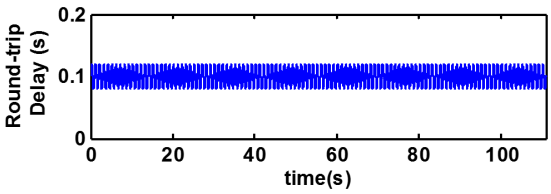

Figure 11. Round-trip Communication Delay

This stabilizer observes the passivity characteristics of the patient's hand biomechanics besides those for the reflected therapeutic forces. If the observed non-passivities in the system (which can either be from the therapy terminal or the patient terminal) can be absorbed by the existing passivity resources in the interconnection, the stabilizer does not change the transparency. If the above-mentioned condition is not observed by the controller, the stabilizer tunes the force reflection gate as needed to guarantee the stability of the system according to the stability condition given in (19).

5 Experimental Evaluation of GPS-map Stabilizer

In this section, the proposed GPS-map Stabilizer is implemented and the corresponding performance is experimentally evaluated. For this purpose, the table-top upper-limb robotic rehabilitation device from Quanser Inc. was utilized. The robotic handle was sensorized using two Interlink pressure sensors which registered the grasp pressure of the user. The experimental setup is shown in Fig. 1. The sensors were connected to a PCIe-6320 data acquisition card from National Instruments to read the pressure values. The Real-time Quarc library (from Quanser Inc.) in Matlab/Simulink was used to run the system. The sampling period for running the setup was $1ms$ and for data logging was $10ms$. To account for possible time-varying communication delays (which exist in the case of cloud-based rehabilitation), a variable round trip delay of $\tau(t) = 100 + 20\sin(2\pi t)$ ms was considered as shown in Fig. 11.

In order to evaluate the performance of the stabilizer, the experiment was performed for both a resistive environment (which is a passive viscous force field) and a power-assistive environment (which is a non-passive negatively viscous force field). During the first phase, the power-assistive force field was generated in Matlab/Simulink with an assistive gain of $20N.s/m$. During the second phase of the experiment, a resistive viscous force field was generated having a viscous gain of $-20N.s/m$. It should be noted that while a resistive environment is a passive component of the system, because of the existence of the communication delays, it can realize a non-passive interconnection such as the assistive environment. As a result, both of the above-mentioned environments can challenge interaction stability, as shown in the results.

5.1 Power Assistive Force Field

In the first phase, the stabilizer was evaluated for power assistive environment, in four steps. For the first three steps the controller was turned on. During the first step ($t \leq 28\ s$), some sudden sharp disturbances were applied to the robot when the user was not holding the robotic handle (zero grasp pressure). In this situation, the stabilizer was considerably challenged since no dissipation was applied by the user's hand. The velocity and force trajectories can be seen in Figs. 12(a), 12(b), and 12(c), when $t \leq 28\ s$. As shown in these figure, the controller was able to stabilize the system and the robot behaved in a safe manner and the trajectories quickly converged to zero after the disturbances were applied. In fact, using the identified GPS map of the user's hand and the measured grasp pressure, the calculated EOP was zero while the nonpassive assistive therapy was being applied. Consequently, the controller was automatically activated to damp out the energy and stabilize the system.

In the second step ($28s \leq t \leq 50s$), the user provided a soft grasp while moving the robot in 2 degrees of freedom. In this step, since the user provided some grasp pressure, the calculated EOP was not zero and the controller allowed part of the non-passive energy to be delivered to the user's hand since it could be partially absorbed by it. The force and motion trajectories are shown in Figs. 12(a), 12(b), and 12(c), for $28s \leq t \leq 50s$. As can be seen in Figs. 12(a) and 12(b), the controller has modified the delivered force to guarantee stability. In addition, the power modification is shown in Fig. 12(d). As shown in the figure, during this step, since the amplitude of the received power packets (solid blue line) was higher that the power that could be absorbed by the user's hand (solid green line), the controller has modified the energy (solid red line) through force modification. As a result, the user could feel the assistive nonpassive forces in the same direction as that of the delivered forces, while the amplitude was modified based on the knowledge of the energy absorption capability of the user's hand. The corresponding grasp pressure is shown in Fig. 12(e), when $28\ s \leq t \leq 50\ s$.

In the third step of this experiment, the user provided higher grasp pressure (shown in Fig. 12(e), when $t > 50s$) while moving the robot in 2 DOF. In this situation, the amplitude of the power absorption capability of the user's hand was higher than the delivered non-passive assistive power (this can be seen in Fig. 12(d) when $t > 50s$). Consequently, the controller allowed all the non-passive power to be reflected back to the user's hand without sacrificing the stability of the system, as shown in Fig. 12(d) for $t > 50s$. As a result, the user was able to feel all the assistive forces (shown in Figs. 12(a) and 12(b) when $t > 50s$) since the controller did not change the reflected nonpassive forces/power and the transparency of the system is completely preserved despite the existence of communication delays and nonpassive assistive environment.

Note that the system behaved in a stable manner during all three steps when the controller was turned on. In the fourth step of the first phase, the controller was turned off and the user tried to gently move the robotic handle. The force and velocity trajectories are shown in Fig. 13. As shown in Fig. 13, once the user touched the robot, the system became unstable and went out-of-control. The trajectories grew in an exponential manner and the robot slammed into the boundary of the workspace.

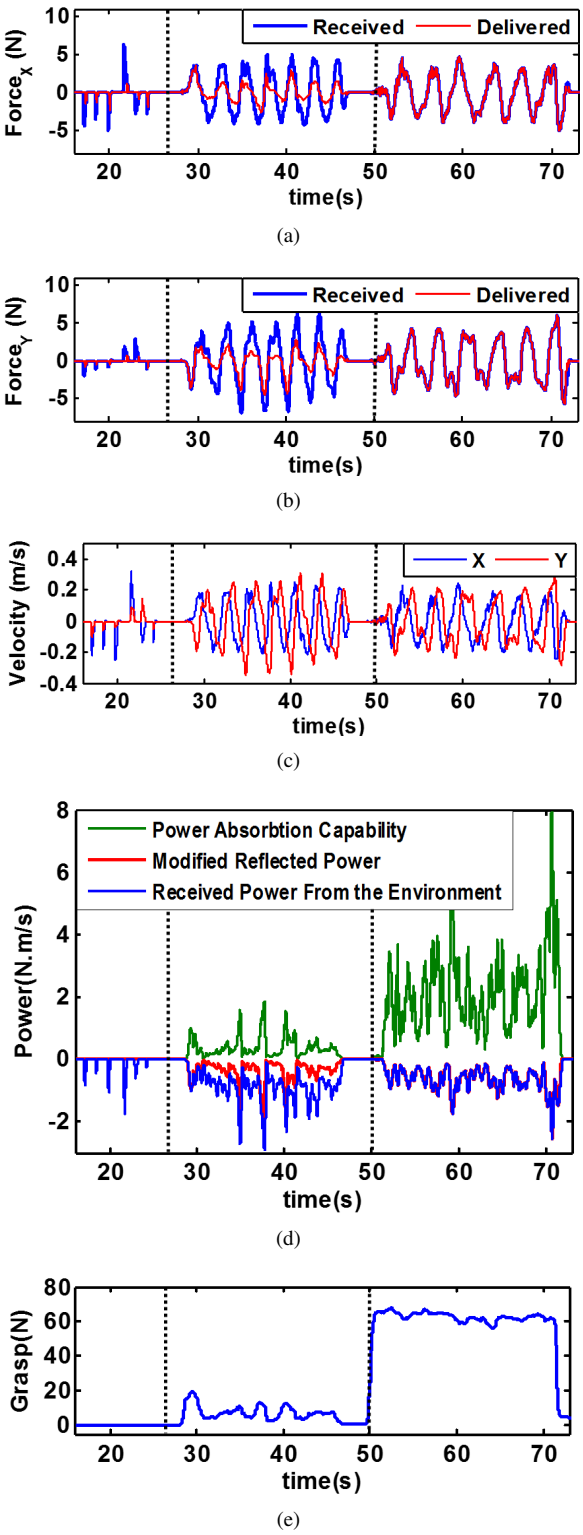

Figure 12. The controller is turned on: (a) the received force at the user's side versus the modified force in the X-direction, (b) the force trajectories in the Y-direction, (c) the velocity trajectories, (d) the power trajectories, (e) the grasp pressure.

5.2 Resistive Viscous Force Field

In the second phase of the experiment, the stabilizing behavior of the controller is shown for the delayed resistive

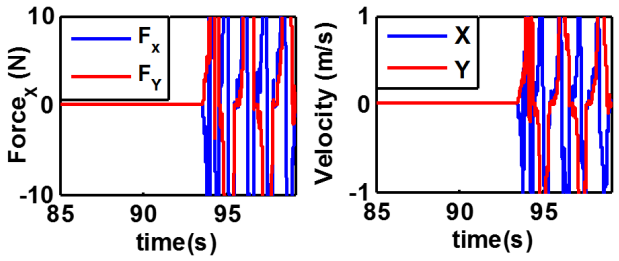

Figure 13. The controller is turned off: (left) the force trajectories, (right) the velocity trajectories.

viscous environment. Similar four steps (conducted for phase 1) have been tested for phase 2. In the first three steps ($t < 75s$), the controller was turned on and different disturbances, motion trajectories and grasp pressures were applied to the robotic handle. The corresponding motion (velocity and position) trajectories are shown in Fig. 14, when $t < 75s$. As can be seen in Fig. 14, during the first three steps, the system behaved in a completely stable manner. In addition, the grasp pressure and the power modification are shown in Figs. 15(a) and 15(b), respectively.

In the forth step, the controller was turned off and the user provided gentle movement that resulted in instability in the form of out-of-control high-frequency diverging oscillations. The corresponding motion profiles are shown in Fig. 14, when $t > 75s$. Due to the intense instability, the mechanical transmission cable of the robot broke.

The results shown in this section, validate the performance of the proposed technique and illustrate that the GPS-map Stabilizer can guarantee stability and interconnection safety based on the real-time estimate of the capability of the user's hand biomechanics in absorbing interaction energies in different directions of interaction. If the user provides enough energy absorption, the controller does not change the reflected forces and allows the non-passive energy to be completely delivered. This results in a perfectly stable and transparent system in the presence of communication delays and a non-passive environment.

6 Conclusion

In this paper, Grasp-based Passivity Signature (GPS) of the human upper-limb was studied in the context of the strong passivity theorem. The proposed GPS map provides a graphical tool to assess and analyze the capability of a user's hand in absorbing interaction energies. For this purpose, a user study was conducted consisting of 11 participants to analyze their arm's and wrist's (both right and left) excess of passivity (EOP), with respect to changes in grasp pressure and geometry of interaction. It was shown that there is a statistically-significant correlation between the change in EOP and (a) the provided grasp pressure, (b) the geometry of interaction. Further statistical investigations may shed more light on different characteristics of the proposed GPS map. Some interesting research questions are the following: "Does the GPS map have a typical shape?", "Is there any similarity between the shape for right and left hands?", "Does human handedness affect the shape of the map?", and "How do gender, age and disabilities affect the shape of the map?". In this paper, GPS map was proposed for the first time

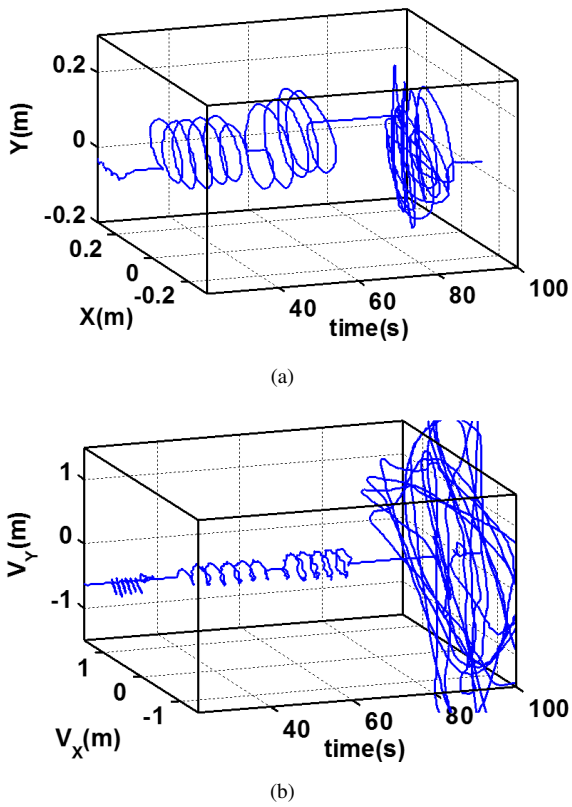

(a)

(b)

Figure 14. Motion trajectories for the case of a viscous environment: (a) 2D position over time, (b) 2D velocity over time.

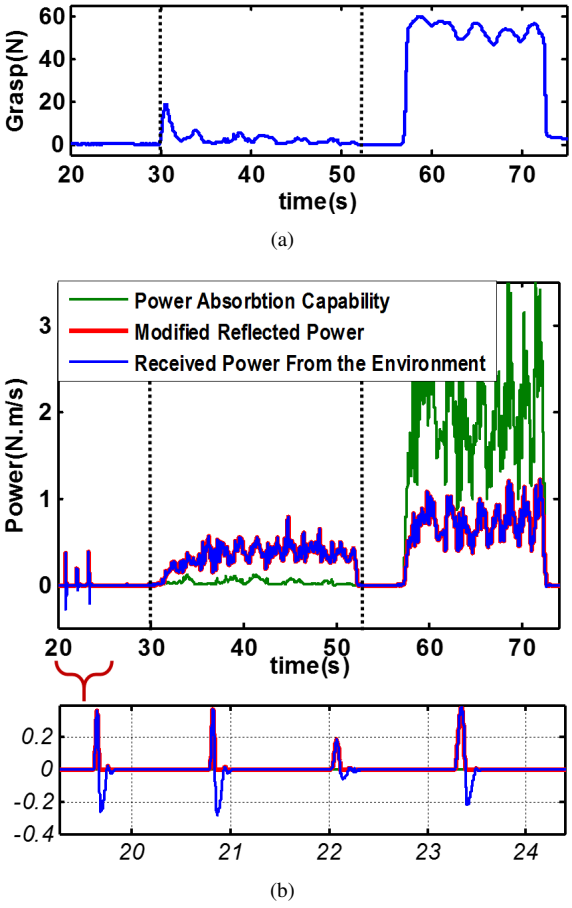

(a)

(b)

Figure 15. The controller is turned on (second phase): (a) the grasp pressure, (b) the power trajectories.

and used in the design of a new controller called the GPS-map Stabilizer. The controller was shown to be capable of guaranteeing human-robot interaction safety through the use of the proposed GPS map. The stabilizer was motivated by application in haptics-enabled rehabilitation technologies where special attention needs to be paid to ensure patient-robot interaction safety. The proposed theory can also be used for conventional haptic and haptic teleoperation systems. The goal of the proposed stabilizer was to minimize transparency distortion using knowledge of the capabilities of the human upper limb in absorbing energy and changes in this capability due to a variable grasp pressure. The stabilizer behaves like a force reflection gate which is completely open if a user provides enough EOP, but otherwise closed just enough to ensure stability. Statistical evaluation and experimental results were reported in support of the proposed technique and the developed theory.

Acknowledgements

This research was supported by the Natural Sciences and Engineering Research Council (NSERC) of Canada and Canadian Institutes of Health Research (CIHR) under a Collaborative Health Research Projects (CHRP) Grant #316170, an AGE-WELL Network of Centres of Excellence Grant AW CRP 2015-WP5.3, the Canada Foundation for Innovation (CFI) under grant LOF 28241, NSERC Discovery Grant RGPIN 1345, the Alberta Innovation and Advanced Education Ministry under Small Equipment Grant RCP-12-021, and Quanser Inc.

References

Aguirre-Ollinger, G., Colgate, J. E., Peshkin, M. A., and Goswami, A. (2012). Inertia compensation control of a one-degree-of-freedom exoskeleton for lower-limb assistance: initial experiments. *Neural Systems and Rehabilitation Engineering, IEEE Transactions on*, 20(1):68–77.

Albu-Schäffer, A., Ott, C., and Hirzinger, G. (2007). A unified passivity-based control framework for position, torque and impedance control of flexible joint robots. *The International Journal of Robotics Research*, 26(1):23–39.

Atashzar, S. F., Polushin, I., and Patel, R. V. (2014a). A small-gain approach for non-passive bilateral telerobotic rehabilitation: Stability analysis and controller synthesis. *submitted to IEEE Transactions on Robotics*.

Atashzar, S. F., Polushin, I. G., and Patel, R. V. (2012a). Networked teleoperation with non-passive environment: Application to tele-rehabilitation. In *IEEE/RSJ International Conference on Intelligent Robots and Systems*, pages 5125–5130.

Atashzar, S. F., Polushin, I. G., and Patel, R. V. (2013). Projection-based force reflection algorithms for teleoperated rehabilitation therapy. In *IEEE/RSJ International Conference on Intelligent Robots and Systems*, pages 477–482.

Atashzar, S. F., Saxena, A., Shahbazi, M., and Patel, R. V. (2014b). Involuntary movement during haptics-enabled robotic rehabilitation: Analysis and control design. In *IEEE/RSJ International Conference on Intelligent Robots and Systems*, pages 3561–3566.

Atashzar, S. F., Shahbazi, M., Samotus, O., Tavakoli, M., Jog, M., and Patel, R. (2016). Characterization of upper-limb pathological tremors: Application to design of an augmented haptic rehabilitation system. *IEEE Journal of Selected Topics in Signal Processing*.

Atashzar, S. F., Shahbazi, M., Talebi, H., and Patel, R. V. (2012b). Control of time-delayed telerobotic systems with flexible-link slave manipulators. In *IEEE/RSJ International Conference on Intelligent Robots and Systems*. IEEE.

Atashzar, S. F., Shahbazi, M., Tavakoli, M., and Patel, R. V. (2015). A new passivity-based control technique for safe patient-robot interaction in haptics-enabled rehabilitation systems. In *Intelligent Robots and Systems (IROS), 2015 IEEE/RSJ International Conference on*, pages 4556–4561. IEEE.

Aziminejad, A., Tavakoli, M., Patel, R. V., and Moallem, M. (2008). Transparent time-delayed bilateral teleoperation using wave variables. *IEEE Transactions on Control Systems Technology*, 16(3):548–555.

Bae, J., Zhang, W., and Tomizuka, M. (2013). Network-based rehabilitation system for improved mobility and tele-rehabilitation. *IEEE Transactions on Control Systems Technology*, 21(5):1980–1987.

Blank, A. A., French, J. A., Pehlivan, A. U., and O'Malley, M. K. (2014). Current trends in robot-assisted upper-limb stroke rehabilitation: promoting patient engagement in therapy. *Current Physical Medicine and Rehabilitation Reports*, 2(3):184–195.

Butler, A., Bay, C., Wu, D., Richards, K., Buchanan, S., et al. (2014). Expanding tele-rehabilitation of stroke through in-home robot-assisted therapy. *International Journal of Physical Medicine & Rehabilitation*, 2(184):2.

Chawda, V. and O'Malley, M. (2015). Position synchronization in bilateral teleoperation under time-varying communication delays. *IEEE/ASME Transactions on Mechatronics*, 20(1):245–253.

Chopra, N., Berestesky, P., and Spong, M. W. (2008). Bilateral teleoperation over unreliable communication networks. *IEEE Transactions on Control Systems Technology*, 16(2):304–313.

Cirstea, M. and Levin, M. F. (2000). Compensatory strategies for reaching in stroke. *Brain*, 123(5):940–953.

Culmer, P. R., Jackson, A. E., Makower, S., Richardson, R., Cozens, J. A., Levesley, M. C., and Bhakta, B. B. (2010). A control strategy for upper limb robotic rehabilitation with a dual robot system. *IEEE/ASME Transactions on Mechatronics*, 15(4):575–585.

De Vlugt, E., de Groot, J. H., Schenkeveld, K. E., Arendzen, J., van der Helm, F. C., and Meskers, C. G. (2010). The relation between neuromechanical parameters and Ashworth score in stroke patients. *Journal of Neuroengineering and Rehabilitation*, 7(1):1.

Dietz, V. and Sinkjaer, T. (2007). Spastic movement disorder: impaired reflex function and altered muscle mechanics. *The Lancet Neurology*, 6(8):725–733.

Dimyan, M. A. and Cohen, L. G. (2011). Neuroplasticity in the context of motor rehabilitation after stroke. *Nature Reviews Neurology*, 7(2):76–85.

Dyck, M. and Tavakoli, M. (2013). Measuring the dynamic impedance of the human arm without a force sensor. In *IEEE International Conference on Rehabilitation Robotics*.

Ellis, M. D., Holubar, B. G., Acosta, A. M., Beer, R. F., and Dewald, J. (2005). Modifiability of abnormal isometric elbow and shoulder joint torque coupling after stroke. *Muscle & Nerve*, 32(2):170–178.

Forbes, J. and Damaren, C. (2010). Passive linear time-varying systems: State-space realizations, stability in feedback, and controller synthesis. In *American Control Conference*, pages 1097–1104.

Haddadin, S., Albu-Schäffer, A., and Hirzinger, G. (2010). Safety analysis for a human-friendly manipulator. *International Journal of Social Robotics*, 2(3):235–252.

Hannaford, B. and Ryu, J.-H. (2002). Time-domain passivity control of haptic interfaces. *IEEE Transactions on Robotics and Automation*, 18(1):1–10.

Hashtrudi-Zaad, K. and Salcudean, S. (2002). Transparency in time-delayed systems and the effect of local force feedback for transparent teleoperation. *IEEE Tranactions on Robotics and Automation*, 18(1):108–114.

Hashtrudi-Zaad, K. and Salcudean, S. E. (2001). Analysis of control architectures for teleoperation systems with impedance/admittance master and slave manipulators. *The International Journal of Robotics Research*, 20(6):419–445.

Herrnstadt, G. and Menon, C. (2016). Voluntary-driven elbow orthosis with speed-controlled tremor suppression. *Frontiers in Bioengineering and Biotechnology*, 4.

Hill, D. J. and Moylan, P. J. (1977). Stability results for nonlinear feedback systems. *Automatica*, 13(4):377–382.

Hogan, N., Krebs, H. I., Rohrer, B., Palazzolo, J. J., Dipietro, L., Fasoli, S. E., Stein, J., Hughes, R., Frontera, W. R., Lynch, D., et al. (2006). Motions or muscles? some behavioral factors underlying robotic assistance of motor recovery. *Journal of Rehabilitation Research and Development*, 43(5):605–618.

Hommel, G., Röhrig, B., and Blettner, M. (2009). Confidence interval or p-value. *Dtsch Arztebl Int*, 106(19):335–339.

Jazayeri, A., Dyck, M., and Tavakoli, M. (2013). Stability analysis of teleoperation systems under strictly passive and non-passive operator. In *World Haptics Conference*, pages 695–700.

Khalil, H. K. and Grizzle, J. (2002). *Nonlinear Systems*, volume 3. Prentice hall, Upper Saddle River.

Kim, H., Miller, L. M., Fedulow, I., Simkins, M., Abrams, G. M., Byl, N., and Rosen, J. (2013). Kinematic data analysis for post-stroke patients following bilateral versus unilateral rehabilitation with an upper limb wearable robotic system. *IEEE Transactions on Neural Systems and Rehabilitation Engineering*, 21(2):153–164.

Krebs, H. I. and Hogan, N. (2006). Therapeutic robotics: A technology push. *Proceedings of the IEEE*, 94(9):1727–1738.

Lee, H. and Hogan, N. (2016). Energetic passivity of the human ankle joint. *IEEE Transactions on Neural Systems and Rehabilitation Engineering*.

Lendvay, T. S., Hannaford, B., and Satava, R. M. (2013). Future of robotic surgery. *The Cancer Journal*, 19(2):109–119.

Makowski, N. S., Knutson, J. S., Chae, J., and Crago, P. E. (2015). Control of robotic assistance using poststroke residual voluntary effort. *IEEE Transactions on Neural Systems and Rehabilitation Engineering*, 23(2):221–231.

Marcus, H. J., Hughes-Hallett, A., Cundy, T. P., Yang, G.-Z., Darzi, A., and Nandi, D. (2015). da vinci robot-assisted keyhole neurosurgery: a cadaver study on feasibility and safety. *Neurosurgical Review*, 38(2):367–371.

Masia, L. and Squeri, V. (2014). A modular mechatronic device for arm stiffness estimation in human-robot interaction. *IEEE/ASME Transactions on Mechatronics*, PP(99):1–14.

McCrea, P. H., Eng, J. J., and Hodgson, A. J. (2003). Linear spring-damper model of the hypertonic elbow: reliability and validity. *Journal of Neuroscience Methods*, 128(1):121–128.

Merians, A. S. and Fluet, G. G. (2014). Rehabilitation applications using virtual reality for persons with residual impairments following stroke. In *Virtual Reality for Physical and Motor Rehabilitation*, pages 119–144. Springer.

Mirbagheri, M. M., Alibiglou, L., Thajchayapong, M., and Rymer, W. Z. (2008). Muscle and reflex changes with varying joint angle in hemiparetic stroke. *Journal of Neuroengineering and Rehabilitation*, 5(1):1.

Morbi, A., Ahmadi, M., Chan, A., and Langlois, R. (2014). Stability-guaranteed assist-as-needed controller for powered orthoses. *IEEE Transactions on Control Systems Technology*, 22(2):745–752.

Niemeyer, G. and Slotine, J.-J. E. (2004). Telemanipulation with time delays. *The International Journal of Robotics Research*, 23(9):873–890.

Okamura, A. M. (2004). Methods for haptic feedback in teleoperated robot-assisted surgery. *Industrial Robot: An International Journal*, 31(6):499–508.

Ryu, J.-H., Kwon, D.-S., and Hannaford, B. (2004). Stability guaranteed control: Time domain passivity approach. *IEEE Transactions on Control Systems Technology*, 12(6):860–868.

Schwamm, L. H., Holloway, R. G., Amarenco, P., Audebert, H. J., Bakas, T., Chumbler, N. R., Handschu, R., Jauch, E. C., Knight, W. A., Levine, S. R., et al. (2009). A review of the evidence for the use of telemedicine within stroke systems of care- A Scientific Statement from the American Heart Association/American Stroke Association. *Stroke*, 40(7):2616–2634.

Seltman, H. J. (2012). Experimental design and analysis. *Online at: http://www. stat. cmu. edu/, hseltman/309/Book/Book. pdf*.

Sethi, A., Davis, S., McGuirk, T., Patterson, T. S., and Richards, L. G. (2013). Effect of intense functional task training upon temporal structure of variability of upper extremity post stroke. *Journal of Hand Therapy*, 26(2):132–138.

Simorov, A., Otte, R. S., Kopietz, C. M., and Oleynikov, D. (2012). Review of surgical robotics user interface: what is the best way to control robotic surgery? *Surgical Endoscopy*, 26(8):2117–2125.

Sun, D., Naghdy, F., and Du, H. (2014). Application of wave-variable control to bilateral teleoperation systems: A survey. *Annual Reviews in Control*, 38(1):12–31.

Taheri, B., Case, D., and Richer, E. (2015). Adaptive suppression of severe pathological tremor by torque estimation method. *IEEE/ASME Transactions on Mechatronics*, 20(2):717–727.

Takeuchi, N. and Izumi, S.-I. (2013). Rehabilitation with poststroke motor recovery: a review with a focus on neural plasticity. *Stroke Research and Treatment*, 2013.

Tavakoli, M., Aziminejad, A., Patel, R. V., and Moallem, M. (2007). High-fidelity bilateral teleoperation systems and the effect of multimodal haptics. *IEEE Transactions on Systems, Man, and Cybernetics, Part B: Cybernetics*, 37(6):1512–1528.

Tavakoli, M., Patel, R., and Moallem, M. (2005). Haptic interaction in robot-assisted endoscopic surgery: a sensorized end-effector. *The International Journal of Medical Robotics and Computer Assisted Surgery*, 1(2):53–63.

Thibaut, A., Chatelle, C., Ziegler, E., Bruno, M.-A., Laureys, S., and Gosseries, O. (2013). Spasticity after stroke: physiology,

assessment and treatment. *Brain Injury*, 27(10):1093–1105.

Tsuji, T., Morasso, P. G., Goto, K., and Ito, K. (1995). Human hand impedance characteristics during maintained posture. *Biological Cybernetics*, 72:475–485.

Vidyasagar, M. (2002). *Nonlinear Systems Analysis*, volume 42. SIAM.

Vitiello, N., Lenzi, T., Roccella, S., De Rossi, S. M., Cattin, E., Giovacchini, F., Vecchi, F., and Carrozza, M. (2013). Neuroexos: A powered elbow exoskeleton for physical rehabilitation. *IEEE Transactions on Robotics*, 29(1):220–235.

Westebring-Van Der Putten, E., Goossens, R., Jakimowicz, J., and Dankelman, J. (2008). Haptics in minimally invasive surgery–a review. *Minimally Invasive Therapy & Allied Technologies*, 17(1):3–16.

Zhang, J. and Cheah, C. C. (2015). Passivity and stability of human–robot interaction control for upper-limb rehabilitation robots. *IEEE Transactions on Robotics*, 31(2):233–245.